

---

# Extensions of fiber bundle models

F. Kun<sup>1</sup>, F. Raischel<sup>2</sup>, R. C. Hidalgo<sup>3</sup>, and H. J. Herrmann<sup>2</sup>

<sup>1</sup> Department of Theoretical Physics, University of Debrecen, P. O. Box:5, H-4010 Debrecen, Hungary [feri@ntp.atomki.hu](mailto:feri@ntp.atomki.hu)

<sup>2</sup> Institute for Computational Physics, University of Stuttgart, Pfaffenwaldring 27, D-70569 Stuttgart, Germany

<sup>3</sup> Department of Fundamental Physics, University of Barcelona, Franques 1, 08028 Barcelona, Spain

The fiber bundle model is one of the most important theoretical approaches to investigate the fracture and breakdown of disordered media extensively used both by the engineering and physics community. We present the basic construction of the model and provide a brief overview of recent results focusing mainly on the physics literature. We discuss the limitations of the model to describe the failure of composite materials and present recent extensions of the model which overcome these problems making the model more realistic: we gradually enhance the fiber bundle model by generalizing the failure law, constitutive behavior, deformation state and way of interaction of fibers. We show that beyond the understanding of the fracture of fiber reinforced composites, these extensions of the fiber bundle model also address interesting problems for the statistical physics of fracture.

## 1 Introduction

The damage and fracture of disordered materials is a very important scientific and technological problem which has attracted an intensive research over the past decades. One of the first theoretical approaches to the problem was the fiber bundle model introduced by Peires in 1927 to understand the strength of cotton yarns [46]. In his pioneering work, Daniels provided the sound probabilistic formulation of the model and carried out a comprehensive study of bundles of threads assuming equal load sharing after subsequent failures [12]. In order to capture fatigue and creep effects, Coleman proposed a time dependent formulation of the model [7], assuming that the strength of loaded fibers is a decreasing function of time. Later on these early works initiated an intense research in both the engineering [47] and physics [23, 6] communities making fiber bundle models one of the most important theoretical approaches to the damage and fracture of disordered materials.

The development of fiber bundle models encountered two kinds of challenges: on the one hand it is important to work out realistic models of materials failure, which have a detailed representation of the microstructure of the material, the local stress fields and their complicated introduction. Such models make possible to clarify the effect of microscopic material parameters on the macroscopic response of solids. In this context, fiber bundle models served as a starting point to develop more realistic micromechanical models of the failure of fiber reinforced composites widely used by the modern aerospace and automobile industry. Analytical methods and numerical techniques have been developed making possible realistic treatment of even large scale fibrous structures. On the other hand, the damage and fracture of disordered materials addresses several interesting problems also for statistical physics. Embedding the failure and breakdown of materials into the general framework of statistical physics and clarifying its analogy to phase transitions and critical phenomena, still keep scientists fascinated. Here fiber bundle models provide an excellent testing ground of ideas offering also the possibility of analytic solutions.

Fiber bundle models have been introduced to describe materials' degradation and failure, however, due to their simplicity, during the last two decades they also served as a general model of the breakdown of a broad class of disordered systems of many interacting elements subject to various types of external loads. Examples can be mentioned from magnets driven by an applied field [11, 71] through scale-free networks [38, 10] to earthquakes [63, 67] and social phenomena [11].

In this paper first we present the basic formulation of the classical fiber bundle model and briefly summarize the most important recent results obtained on the macroscopic response and microscopic damage process of disordered materials focusing on the physics literature. We discuss limitations of the model to describe the fracture of fiber reinforced composites and propose extensions which make the model more realistic. We gradually improve components of the model construction by generalizing the damage law, constitutive behavior, deformation state and interaction law of fibers. Finally, we give an overview of the applications of the extended fiber bundle model.

## 2 Fiber bundle model of materials failure

The construction of fiber bundle models (FBMs) is based on the following simplifying assumptions [12, 49, 53, 62, 2, 28]:

*Discretization* The disordered solid is represented as a discrete set of parallel fibers of number  $N$  organized on a regular lattice (square, triangular, ...), see Fig. 1. The fibers can solely support longitudinal deformation which allows to study only loading of the bundle parallel to fibers.

*Failure law* When the bundle is subjected to an increasing external load, the fibers are assumed to have perfectly brittle response, *i.e.* they have linearly

elastic behavior until they break at a failure load  $\sigma_{th}^i$ ,  $i = 1, \dots, N$  as it is illustrated in Fig. 2a). The elastic behavior of fibers is characterized by the Young modulus  $E$ , which is identical for all fibers. The failure of fibers is instantaneous and irreversible such that the load on broken fibers drops down to zero immediately at the instant of failure (see Fig. 2a)), furthermore, broken fibers are never restored (no healing).

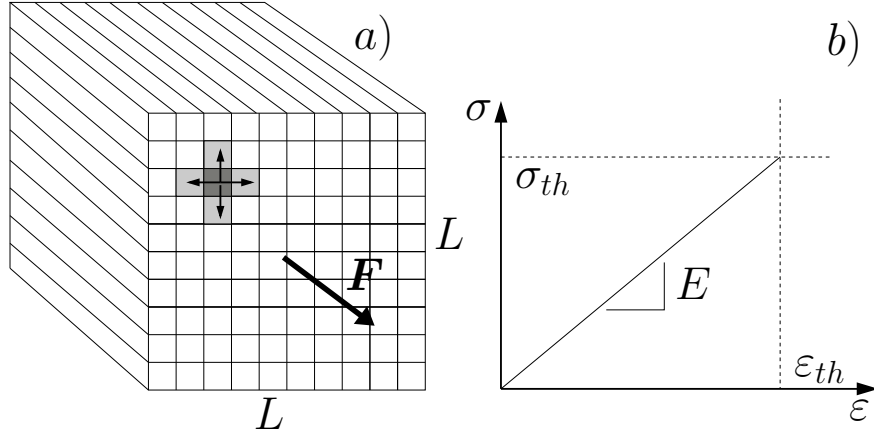


**Fig. 1.** a) Set up of the classical fiber bundle model. Parallel fibers are assembled on a square lattice of size  $L \times L$  loaded by an external force  $F$  parallel to the fiber direction. In the limiting case of very localized load sharing the load of a failed fiber (dark grey) is equally redistributed over its nearest intact neighbors (light grey). b) Single fibers have linearly elastic behavior up to the failure load  $\sigma_{th}$ .

*Load sharing rule* After a fiber fails its load has to be shared by the remaining intact fibers. The range and form of interaction of fibers, also called load sharing rule, is a crucial components of the model which has a substantial effect on the micro and macro behavior of the bundle. Most of the studies in the literature are restricted to two extreme forms of the load sharing rule: (i) in the case of global load sharing (GLS), also called equal load sharing (ELS), the load is equally redistributed over all intact fibers in the bundle irrespective of their distance from the failed one. The GLS rule corresponds to the mean field approximation of FBM where the topology of the fiber bundle (like the square lattice structure in Fig. 2a)) becomes irrelevant. Such a loading condition naturally arises when parallel fibers are loaded between perfectly rigid platens, like for the wire cable of an elevator. FBM with global load sharing is a usual starting point for more complex investigations since it makes possible to obtain the most important characteristic quantities of the bundle in closed analytic forms [28, 22, 54, 53, 62]. (ii) In the other extreme of the local load sharing (LLS), the entire load of the failed fiber is redistributed equally over

its local neighborhood (usually nearest neighbors) in the lattice considered leading to stress concentrations along failed regions (see Fig. 1a)). Due to the non-trivial spatial correlations, the analytic treatment of LLS bundles has serious limitations [17, 49, 20], most of the studies here rely on large scale computer simulations [18, 9, 21, 26]. Such localized load sharing occurs when a bundle of fibers is loaded between plates of finite compliance [19, 4, 13].

*Distribution of failure thresholds* The strength of fibers  $\sigma_{th}^i$ , i.e. the value of the local load at which they break, is an independent identically distributed random variable with the probability density  $p(\sigma_{th})$  and distribution function  $P(\sigma_{th}) = \int_{\sigma_{th}^{min}}^{\sigma_{th}^{max}} p(x)dx$ . The randomness of breaking thresholds is assumed to represent the disorder of heterogeneous materials, and hence, it is practically the only component of the classical FBM where material dependent features (e.g. amount of disorder) can be taken into account. For the disordered breaking thresholds the uniform distribution between 0 and 1 with the density and distribution functions

$$p(\sigma_{th}) = 1, \quad P(\sigma_{th}) = \sigma_{th}, \quad (1)$$

is a usual starting point in most of the investigations. Another widely used distribution in FBMs is the Weibull distribution

$$P(\sigma_{th}) = 1 - \exp \left[ - \left( \frac{\sigma_{th}}{\lambda} \right)^m \right], \quad (2)$$

where  $m$  and  $\lambda$  denote the Weibull index and scale parameter, respectively. Besides its physical ground [23, 6], the Weibull distribution has the advantage from the viewpoint of modelling that the amount of disorder can be controlled by varying the Weibull index  $m$ .

*Time dependence* According to the time dependence of the fiber strength, two classes of FBMs can be distinguished: in static fiber bundles the breaking thresholds are constant during the entire loading history of the bundle. In order to model a certain type of creep rupture and fatigue behavior of materials, time dependent strength of fibers have been introduced [7, 65, 34, 35, 42].

In spite of their simplicity, FBMs provided a deeper understanding of the breakdown of heterogeneous materials revealing important basic features of the failure process. In the following we briefly summarize the most important results of FBMs on the microscopic failure process and macroscopic response of disordered materials under quasistatic loading conditions. Loading of a parallel bundle of fibers can be performed in two substantially different ways: when the deformation  $\varepsilon$  of the bundle is controlled externally the load on single fibers  $\sigma_i$  is always determined by the externally imposed deformation  $\varepsilon$  as  $\sigma_i = E\varepsilon$ , i.e. no load sharing occurs and consequently the fibers break one-by-one in the increasing order of their breaking thresholds. At a given deformation  $\varepsilon$  the fibers with breaking thresholds  $\sigma_{th}^i < E\varepsilon$  are broken, furthermore, all intact fibers keep the equal load  $E\varepsilon$ . Hence, the macroscopic constitutive behavior  $\sigma(\varepsilon)$  of the FBMs can be cast in the form

$$\sigma(\varepsilon) = E\varepsilon [1 - P(E\varepsilon)], \quad (3)$$

where  $[1 - P(E\varepsilon)]$  is the percentage of intact fibers at the deformation  $\varepsilon$  [62, 11]. A representative example of  $\sigma(\varepsilon)$  is presented in Fig. 2b) for the case of Weibull distributed strength values with  $m = 2$  and  $\lambda = 1$ . Under stress controlled conditions when the load is gradually increased externally, a more complex damage process occurs starting with the breaking of the weakest fiber. After each fiber breaking the load dropped by the broken fiber has to be redistributed over the surviving intact ones. Assuming global load sharing (equal load sharing), all intact fibers receive the same load increment which might cause secondary fiber breakings. The subsequent load redistribution after consecutive fiber failures can lead to an entire avalanche of breakings which can stop after a certain number of fibers keeping the integrity of the bundle, or can be catastrophic resulting in the macroscopic failure of the entire system. Hence, under stress controlled loading, the constitutive curve Eq. (3) can only be realized up to the maximum, where a catastrophic avalanche occurs breaking all the remaining fibers [28, 22, 54, 24]. It has been shown analytically that for a broad class of disorder distributions  $P$  under GLS conditions the macroscopic constitutive curve  $\sigma(\varepsilon)$  of FBMs has a quadratic maximum whose position and value define the critical strain  $\varepsilon_c$  and stress  $\sigma_c$  of the bundle [62, 11], respectively (see Fig. 2b)). Increasing the size  $N$  of finite bundles, the global strength  $\sigma_c(N)$  rapidly converges to the finite non-zero strength of the infinite bundle [12, 62, 49].

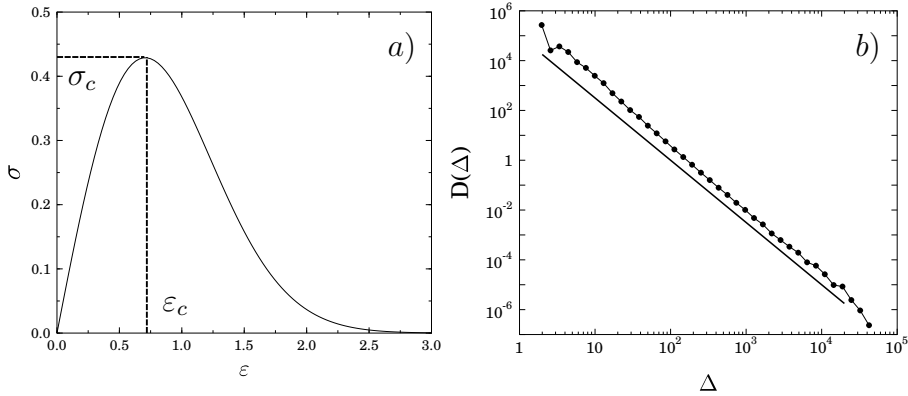


**Fig. 2.** *a)* Macroscopic constitutive behavior of a fiber bundle with global load sharing Eq. (3) using Weibull distributed strength values  $\sigma_{th}$  ( $m = 2$  and  $\lambda = 1$ ). *b)* Distribution  $D$  of burst sizes  $\Delta$  obtained by computer simulations of a bundle of  $10^7$  fibers. A straight line of slope 2.5 is drawn to guide the eye.

When the load sharing is localized the macroscopic response of the bundle becomes more brittle, i.e. the constitutive curve  $\sigma(\varepsilon)$  of the LLS bundle follows its GLS counterpart but the macroscopic failure occurs at a lower critical stress  $\sigma_c^{LLS} < \sigma_c^{GLS}$ , which is preceded by only a weak non-linearity [26]. Large scale computer simulations revealed that in the thermodynamic limit  $N \rightarrow \infty$ , the strength of LLS bundles tends to zero as  $1/(\ln N)$ .

On the micro-level the spatial and temporal evolution of damage shows also a strong dependence on the range of load redistribution: when the excess load of failed fibers is redistributed globally (GLS) no spatial correlations arise, i.e. fiber breaking proceeds in a completely stochastic manner in space which results in randomly nucleated clusters of broken fibers analogous to percolation. Under stress controlled loading conditions, the subsequent load redistribution results in a bursting activity preceding the macroscopic failure of the bundle. For equal load sharing it has been proven analytically that the distribution  $D(\Delta)$  of burst sizes  $\Delta$  recorded during the entire course of loading has a universal power law behavior

$$D(\Delta) \sim \Delta^{-\alpha}, \quad (4)$$

with an exponent  $\alpha = 5/2$  independent of the disorder distribution  $P$  [28, 22, 51]. The power law distribution of bursts prevails also for more complicated long range interactions (like in the fuse model [3, 45]) but localized load sharing results in a rapid decrease of  $D(\Delta)$  and in a dependence on the specific form of disorder  $P$  [18].

In recent years several novel aspects of breakdown phenomena have been revealed in the framework of FBMs: It has been shown that thermal noise leads to the reduction of the strength of materials, furthermore, thermally activated cracking gives rise to sub-critical crack growth and a finite lifetime of materials [59, 61]. When avalanches of fiber failures are solely recorded in the vicinity of the point of macroscopic failure, *i.e.* the strength distribution of the remaining intact fibers is close to critical, the avalanche size distribution  $D(\Delta)$  proved to show a crossover from the power law of exponent  $5/2$  to another power law regime with a lower exponent  $3/2$  [55, 56]. The connectivity properties of the bundle turned out to play an important role in breakdown processes, *i.e.* determining the local interacting partners of fibers in a bundle by a Barabasi-Albert network instead of a regular lattice, the failure process is substantially different [10].

FBMs played also a crucial role to clarify the fundamental problem of the relation of breakdown of disordered materials to critical phenomena [71, 69, 5, 68, 2, 37] and self organized criticality [36]. When fiber bundles with global load sharing approach the point of macroscopic failure under a quasistatically increasing load, it was found that microscopic quantities of the bundle such as the distribution of bursts of fiber breakings show a scaling behavior typical for continuous phase transitions [19, 28, 22, 37, 5, 53, 52, 51]. Since at the same time macroscopic quantities like the Young modulus of the bundle proved to have a finite jump, it was suggested that the macroscopic failure of GLS

systems occurs analogous to first order phase transitions close to a spinodal [70, 71, 69, 33]. An interesting mapping of the fracture process of fiber bundles to Ising-like models widely studied in statistical physics has been suggested [57, 66, 53], which provides further hint to embed fracture phenomena into the general framework of statistical physics.

## 2.1 Why extensions are necessary?

A very important type of materials for which fiber bundle models are of outstanding importance are the so-called fiber reinforced composites (FRC) which have two ingredients, *i.e.* a matrix or carrier material in which thin fibers of another material are embedded in a certain geometrical arrangement. The modern automotive and aerospace industry use a large amount of fiber reinforced composites due to their very good mass specific properties, *i.e.* FRCs provide a very high strength at a relatively low mass and they sustain these properties also under extreme conditions (high temperature, pressure). The mechanical performance of FRC can be well controlled by the properties of the fiber and matrix materials, and by the fabrication of the fiber-matrix interface and the geometrical structure of the composite. This flexibility makes possible the design and tailoring of special purpose structural materials that best fit to the demands of applications. Fig. 3a) presents the structure of the carbon fiber reinforced silicon carbide composite (C/C-SiC) extensively used by the aerospace industry. It can be observed that parallel bundles of long carbon fibers (diameter  $\sim 10\mu m$ ) are embedded in the silicon-carbide ceramic matrix [30]. Reinforcement by fibrous structures can also be found in nature in various types of plants. The structure of soft-wood of the spruce is shown in Fig. 3b) as a representative example [15]. Theoretical studies of the fracture of composites encounter various challenges: on the one hand, applications of materials in construction components require the development of analytical and numerical models which are able to predict the damage histories of loaded specimens in terms of the characteristic microscopic parameters of the constituents. On the other hand, it is important to reveal universal aspects of the fracture of composites, which are independent of specific material properties relevant on the microlevel. Such universal quantities can help to extract the relevant information from measured data and make possible to design monitoring techniques of the gradual degradation of composites' strength and construct methods of forecasting catastrophic failure events.

When fiber composites are subject to an external load parallel to the fiber direction, most of the load is carried by the fibers, the matrix material and properties of the fiber-matrix interface mainly determine the interaction (load transfer) among fibers, which make FBMs the most adequate approach to describe the fracture process of FRCs [48, 50, 8, 30]. As it has been presented above, in their basic setup FBMs provide a rather idealized representation of the behavior of disordered brittle materials. In order to obtain a more realistic description especially for the failure of composites, FBMs have to be

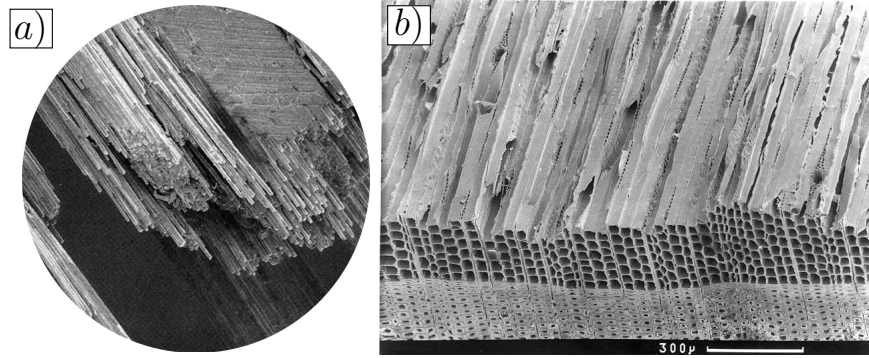


**Fig. 3.** *a)* Structure of a fiber reinforced composite (Carbon fiber reinforced silicon-carbide). Long parallel fibers are embedded in a matrix material [30]. *b)* The softwood is an example of natural fibrous materials. The fibers are tubes whose wall gets thicker with time [15].

enhanced by capturing a more detailed picture of the mechanical behavior of the constituents, the evolution of the local stress field and its interaction with the disordered material properties. In the following we outline important aspects of the mechanical performance of FRCs which cannot be described in the framework of the classical FBM but call for extensions of the model.

In applications, long fiber composites loaded parallel to the direction of fibers are often found to undergo a gradual degradation process such that the macroscopic constitutive curve  $\sigma(\varepsilon)$  of the composite develops a plateau regime and the global failure is preceded by strain hardening. This effect becomes especially important when the fiber bundle has a hierarchical organization and the failure mechanisms relevant at the lower length scales (at the scale of fibers) gradually activate the breaking of higher order substructures (sub-bundles, bundles, and plies) of the system. When fibers are embedded in a matrix material, after a fiber breaks, the fiber-matrix interface debonds in the vicinity of the crack [49]. Due to the frictional contact at the interface, the load of failed fibers builds up again over a certain stress recovery length so that the broken fiber can still contribute to the overall load bearing capacity of the system.

Under high steady stresses, materials may undergo time dependent deformation resulting in failure called creep rupture, which determines the long time performance and limits the lifetime of construction elements. This complex time dependent macroscopic behavior emerges as the result of the interplay of the time dependent deformation of the constituents and the gradual accumulation of damage.

In applications solid blocks are often joined together by welding or gluing of the interfaces which are expected to sustain various types of exter-

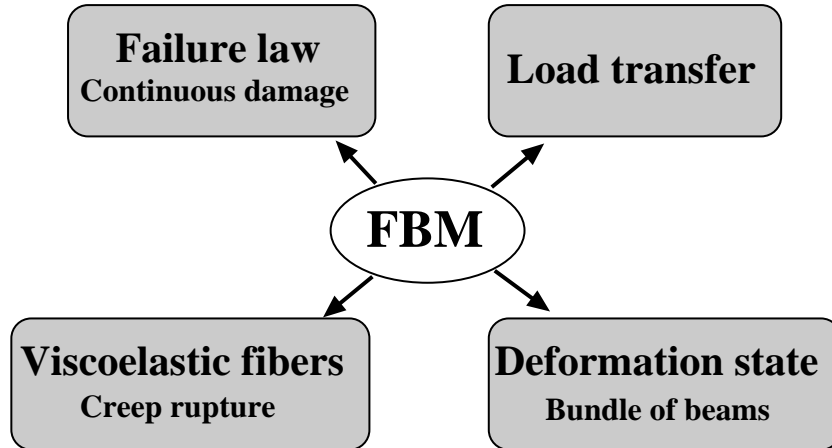


**Fig. 4.** Extensions of fiber bundle models: we gradually enhance FBMs by generalizing the damage law, the load transfer, the constitutive behavior and deformation state of the fibers.

nal loads. Interfacial failure also occurs in fiber reinforced composites, where debonding of the fiber-matrix interface can even be the dominating damage mechanism when the composite is sheared. When interfaces of solids are subject to shear the interface elements suffer not only longitudinal deformation (compression and elongation) but also bending deformation. Such complex deformation states cannot be captured by discretizing the interface in terms of fibers which can only support longitudinal deformation.

As it has been discussed in Sec. 2, the range and functional form of load redistribution of fibers play a crucial role in the failure process of the model. A realistic description of load transfer following fiber failure should obviously fall somewhere between the limiting cases of the widely studied global and local load redistributions. The importance of the accurate description of the load transfer from broken to intact fibers has already been recognized by Daniels for cotton yarns [12].

In the following we present extensions of the classical fiber bundle model gradually improving components of the model construction outlined in Sec. 2: *(I)* In order to understand the damage mechanism that lead to plateau formation and strain hardening of the macroscopic response of quasi-brittle materials, we modify the failure law of fibers in FBMs assuming that individual fibers undergo a gradual degradation process reducing their Young modulus in a multiplicative way in consecutive failure events. *(II)* To describe the damage enhanced creep of fibrous materials we introduce time dependent deformation behavior for the fibers and combine it with strain controlled breaking in a global load sharing framework. *(III)* We show that more complex deformations states (besides the longitudinal deformation) and failure

processes can be described by FBMs when fibers are substituted by beams, which can be stretched, compressed and bent at the two ends. We apply the bundle of beams to investigate the fracture of glued interfaces of solid blocks. (IV) Motivated by the results of fracture mechanics on the stress distribution around cracks, we introduce a one-parameter load transfer function for fibers, which can interpolate between the limiting cases of global and local load sharing. The value of the parameter of the load transfer function controls the effective range of interaction of broken and intact fibers. We apply the variable range of load sharing approach also to clarify universal aspects of the creep rupture of composites. Fig. 4 gives an overview of the structure of the remaining part of the paper. We note that since in the framework of the classical fiber bundle model no effect of the matrix material between fibers is taken into account, the model is also called dry fiber bundle model (DFBM) in the literature in order to distinguish it from the improved variants.

### 3 Gradual degradation of fiber strength

In the following we introduce a so-called continuous damage fiber bundle model as an extension of the classical FBM by generalizing the damage law of fibers. We assume that the stiffness of fibers gradually decreases in consecutive failure events. We show that varying its parameters, the model provides a broad spectrum of macroscopic constitutive behaviors from plasticity to strain hardening in qualitative agreement with experiments. To reveal the microscopic process of damage we construct a simulation techniques and obtain the statistics of bursts of fiber breakings. We find that burst distributions show a power law behavior but surprisingly the exponent can be different from the well know mean field exponent of FBMs [33, 24].

#### 3.1 Continuous damage fiber bundle model

Based on the classical fiber bundle model, the continuous damage model is composed of  $N$  parallel fibers with identical Young-modulus  $E$  and random failure thresholds  $\sigma_{th}^i$ ,  $i = 1, \dots, N$  of probability density  $p$  and distribution function  $P$  (see also Fig. 1 for illustration). The fibers are assumed to have linear elastic behavior up to breaking (brittle failure). Under uniaxial loading of the specimen a fiber fails if it experiences a load larger than its breaking threshold  $\sigma_{th}^i$ . We generalize the failure law of DFBM by assuming that at the failure point the stiffness of the fiber gets reduced by a factor  $a$ , where  $0 \leq a < 1$ , *i.e.* the stiffness of the fiber after failure is  $aE$ . In principle, a fiber can now fail more than once and the maximum number  $k_{max}$  of failures allowed for fibers is a parameter of the model. Once a fiber has failed, its damage threshold  $\sigma_{th}^i$  can either be kept constant for the further breakings (quenched disorder) or new failure thresholds of the same distribution can be chosen (annealed disorder), which can model some microscopic rearrangement

of the material after failure. The damage law of the model is illustrated in Fig. 5 for both types of disorder, which should be compared to Fig. 1. The characterization of damage by a continuous parameter corresponds to describe the system on length scales larger than the typical crack size. This can be interpreted such that the smallest elements of the model are fibers and the continuous damage is due to cracking inside fibers. However, the model can also be considered as the discretization of the system on length scales larger than the size of single fibers, so that one element of the model consists of a collection of fibers with matrix material in between. In this case the microscopic damage mechanism resulting in multiple failure of the elements is the gradual cracking of matrix and the breaking of fibers. In the following we refer to the elements of the continuous damage FBM as fibers, but we have the above two possible interpretations in mind. After failure the fiber skips a

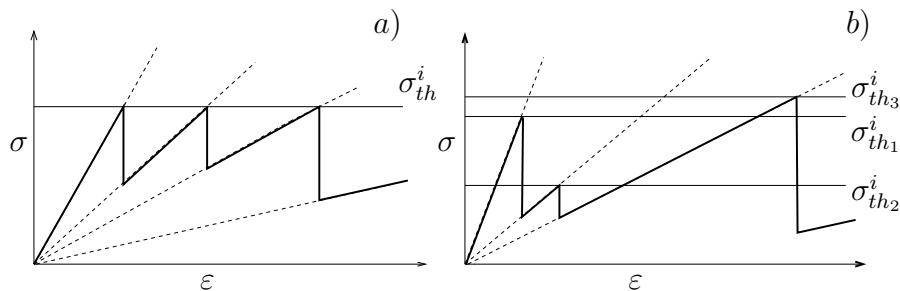


**Fig. 5.** The damage law of a single fiber of the continuous damage model when multiple failure is allowed *a*) for quenched, and *b*) for annealed disorder. The horizontal lines indicate the damage threshold  $\sigma_{th}^i$ . See also Ref. [33, 24].

certain amount of load which has to be taken by the other fibers. For the load redistribution we assume infinite range of interaction among fibers (mean field approach), furthermore, equal strain condition is imposed which implies that stiffer fibers of the system carry more load. At a strain  $\varepsilon$ , the load of fiber  $i$  that has failed  $k(i)$  times reads as

$$f_i(\varepsilon) = Ea^{k(i)}\varepsilon, \quad (5)$$

where  $Ea^{k(i)}$  is the actual stiffness of fiber  $i$ . It is important to note that, in spite of the infinite interaction range, Eq. (5) is different from the usual global load sharing (GLS) where all the intact fibers carry always the same amount of load (see Sec. 2). In the following the initial fiber stiffness  $E$  will be set to unity.

### 3.2 Macroscopic constitutive behavior

The key quantity to determine the macroscopic constitutive behavior of the continuous damage fiber bundle model (CDFBM) and to characterize its mi-

crossopic damage process, is the probability  $P_k(\varepsilon)$  that during the loading of a specimen an arbitrarily chosen fiber failed precisely  $k$ -times at a strain  $\varepsilon$ . Here  $k = 0, \dots, k_{max}$  denotes the failure index, and  $k = 0$  is assigned to the intact fibers.  $P_k(\varepsilon)$  can be cast in the following form for *annealed disorder*

$$P_k(\varepsilon) = [1 - P(a^k \varepsilon)] \prod_{j=0}^{k-1} P(a^j \varepsilon), \quad (6)$$

for  $0 \leq k \leq k_{max} - 1$ ,

and  $P_{k_{max}}(\varepsilon) = \prod_{j=0}^{k_{max}-1} P(a^j \varepsilon)$ ,

and for *quenched disorder*

$$\begin{aligned} P_0(\varepsilon) &= 1 - P(\varepsilon), \\ P_k(\varepsilon) &= P(a^{k-1} \varepsilon) - P(a^k \varepsilon), \text{ for } 1 \leq k \leq k_{max} - 1, \\ \text{and } P_{k_{max}}(\varepsilon) &= P(a^{k_{max}-1} \varepsilon). \end{aligned} \quad (7)$$

It can easily be seen that the probabilities Eqs. (6,7) fulfill the normalization condition  $\sum_{k=0}^{k_{max}} P_k(\varepsilon) = 1$ . Average quantities of the fiber ensemble during a loading process can be calculated using the probabilities Eqs. (6,7). For instance, the average load on a fiber  $F/N$  at a given strain  $\varepsilon$  reads as

$$\frac{F}{N} = \varepsilon \left[ \sum_{k=0}^{k_{max}} a^k P_k(\varepsilon) \right], \quad (8)$$

which provides the macroscopic constitutive behavior of the model. The single terms in the sum give the load carried by the subset of fibers of failure index  $k$ . The variants of fiber bundle models used widespread in the literature can be recovered by special choices of the parameters  $k_{max}$  and  $a$  of the model. A micromechanical model of composites [48, 50, 8, 30] can be obtained with the parameter values  $k_{max} = 1$ ,  $a \neq 0$

$$\frac{F}{N} = \varepsilon [1 - P(\varepsilon)] + a\varepsilon P(\varepsilon), \quad (9)$$

while setting  $k_{max} = 1$ ,  $a = 0$ , *i.e.* skipping the second term in Eq. (9) results in the classical dry bundle model of Daniels [12] with the constitutive behavior Eq. (3). In Fig. 6 we show the explicit form of the constitutive law with annealed disorder for different values of  $k_{max}$  in the case of the Weibull distribution Eq. (2). The parameter values are set to  $m = 2$ ,  $\lambda = 1$  in all the calculations.

Note that in the constitutive equation Eq. (8) the term of the highest failure index  $k_{max}$  can be conceived such that the fibers have a residual stiffness of  $a^{k_{max}}$  after having failed  $k_{max}$  times. This residual stiffness results in a

hardening of the material, hence, the  $F/N$  curves in Fig. 6(a) asymptotically tend to straight lines with a slope  $a^{k_{max}}$ . Increasing  $k_{max}$  the hardening part of the constitutive behavior is preceded by a longer and longer plastic plateau, and in the limiting case of  $k_{max} \rightarrow \infty$  the materials behavior becomes completely plastic. A similar plateau and asymptotic linear hardening has been observed in brittle matrix composites, where the multiple cracking of matrix turned to be responsible for the relatively broad plateau of the constitutive behavior, and the asymptotic linear part is due to the linear elastic behavior of fibers remained intact after matrix cracking [16].

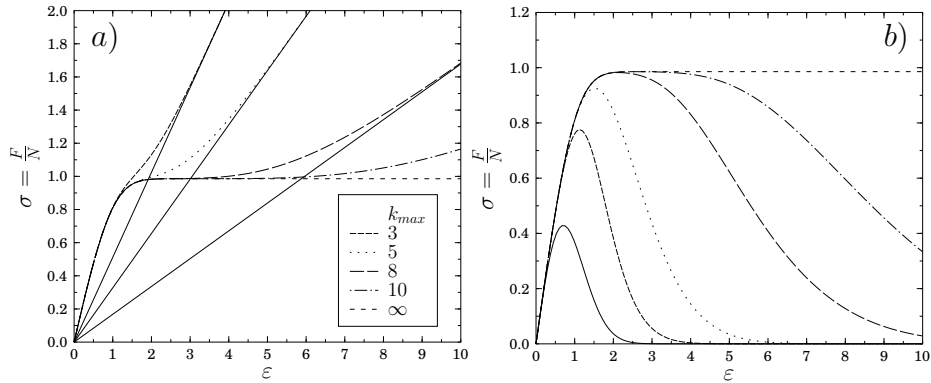


**Fig. 6.** Constitutive behavior of the model of annealed disorder *a)* with *b)* without residual stiffness at  $a = 0.8$  for different values of  $k_{max}$ . In *b)* the lowest curve presents the constitutive behavior of the classical dry bundle model for comparison.

In order to describe macroscopic cracking and global failure of a specimen instead of hardening, the residual stiffness of the fibers has to be set to zero after a maximum number  $k^*$  of allowed failures [33, 72]. In this case the constitutive law can be obtained from the general form Eq. (8) by replacing  $k_{max}$  in the upper limit of the sum by  $k^* - 1$ . A comparison of the constitutive laws of the dry and continuous damage FBM with global failure is presented in Fig. 6(b). One can observe that the dry FBM constitutive law has a relatively sharp maximum, while the continuous damage FBM curves exhibit a plateau whose length increases with increasing  $k^*$ . Note that the maximum value of  $F/N$  corresponds to the macroscopic strength of the material, furthermore, in stress controlled experiments the plateau and the decreasing part of the curves cannot be reached. However, by controlling the strain  $\varepsilon$ , the plateau and the decreasing regime can also be realized. The value of the driving stress  $\sigma \equiv F/N$  corresponding to the plastic plateau, and the length of the plateau are determined by the damage parameter  $a$ , and by  $k_{max}$ ,  $k^*$ : Decreasing  $a$

at a fixed  $k_{max}, k^*$ , or increasing  $k_{max}, k^*$  at a fixed  $a$  give rise to an increase of the plateau's length.

### 3.3 Simulation techniques

Due to the difficulties of the analytic treatment, we develop a simulation technique and explore numerically the properties of bursts of fiber breakings in our continuous damage fiber bundle model. The interaction of fibers, the way of load redistribution is crucial for the avalanche activity. A very important property of CDFBM is that in spite of the infinite range of interaction the load on intact fibers is not equal, but stiffer fibers carry more load, furthermore, for quenched disorder damage localization occurs, which might affect also the avalanche activity [33, 24].

To implement the quasi-static loading of a specimen of  $N$  fibers in the framework of CDFBM, the local load on the fibers  $f_i$  has to be expressed in terms of the external driving  $F$ . Making use of Eq. (5) it follows that

$$F = \sum_{i=1}^N f_i = \varepsilon \sum_{i=1}^N a^{k(i)}, \quad (10)$$

and hence, the strain and the local load on fibers can be obtained as

$$\varepsilon = \frac{F}{\sum_{i=1}^N a^{k(i)}}, \quad f_i = F \frac{a^{k(i)}}{\sum_{i=1}^N a^{k(i)}}, \quad (11)$$

when the external load  $F$  is controlled. The simulation of the quasi-static loading proceeds as follows: in a given stable state of the system we determine the load on the fibers  $f_i$  from the external load  $F$  using Eq. (11). The next fiber to break can be found as

$$r = \frac{\sigma_{th}^{i^*}}{f_{i^*}} = \min_i \frac{\sigma_{th}^i}{f_i}, \quad r > 1, \quad (12)$$

*i.e.* that fiber breaks for which the ratio  $\sigma_{th}^i/f_i$  is the smallest. Here  $i^*$  denotes the index of the fiber to break,  $\sigma_{th}^i$  is the damage threshold of fiber  $i$ , and  $f_i$  is the local load on it. To ensure that the local load of a fiber is proportional to its stiffness, the external load has to be increased in a multiplicative way, so that  $F \rightarrow rF$  is imposed, and the failure index of fiber  $i^*$  is increased by one  $k(i^*) \rightarrow k(i^*) + 1$ . After the breaking of fiber  $i^*$ , the load  $f_i$  carried by the fibers has to be recalculated making use of Eq. (11), which provides also the correct load redistribution of the model. If there are fibers in the state obtained, whose load exceeds the local breaking threshold, they fail, *i.e.* their failure index is increased by 1 and the local load is again recalculated until a stable state is obtained. A fiber cannot break any longer if its failure index  $k$

has reached  $k^*$  or  $k_{max}$  during the course of the simulations. This dynamics gives rise to a complex avalanche activity of fiber breaks, which is also affected by the type of disorder. The size of an avalanche  $\Delta$  is defined as the number of breakings initiated by a single failure due to an external load increment.

### 3.4 Bursts of fibers breakings

Computer simulations revealed that varying the two parameters of the model  $k_{max}$ ,  $a$ , or  $k^*$ ,  $a$  and the type of disorder, the CDFBM shows an interesting variety of avalanche activities, characterized by different shapes of the avalanche size distributions. In Fig. 7a) the histograms  $D(\Delta)$  of the avalanche sizes  $\Delta$  are shown which were obtained for a system of remaining stiffness and annealed disorder with Weibull parameters  $m = 2$ ,  $\lambda = 1$ . Since in the limiting case of  $a \rightarrow 0$  the CDFBM recovers the global load sharing dry fiber bundle model, in Fig. 7a) the curves with small  $a$  and  $k_{max} = 1$  are power laws with an exponent  $\alpha = 5/2$  in agreement with the analytic results [28, 22, 54]. Increasing the value of  $a$  at a fixed  $k_{max}$  only gives rise to a larger number of avalanches, *i.e.* parallel straight lines are obtained on a double logarithmic plot, but the functional form of  $D(\Delta)$  does not change. However, when  $a$  exceeds a critical value  $a_c$  ( $a_c \approx 0.3$  was obtained with the Weibull parameters specified above) the avalanche statistics drastically changes. At a fixed  $a > a_c$  when  $k_{max}$  is smaller than a specific value  $k_c(a)$ , the avalanche sizes show exponential distribution, while above  $k_c(a)$  the distribution takes a power law form with an exponent  $\beta = 2.12 \pm 0.05$ . Based on the above results of simulations a phase

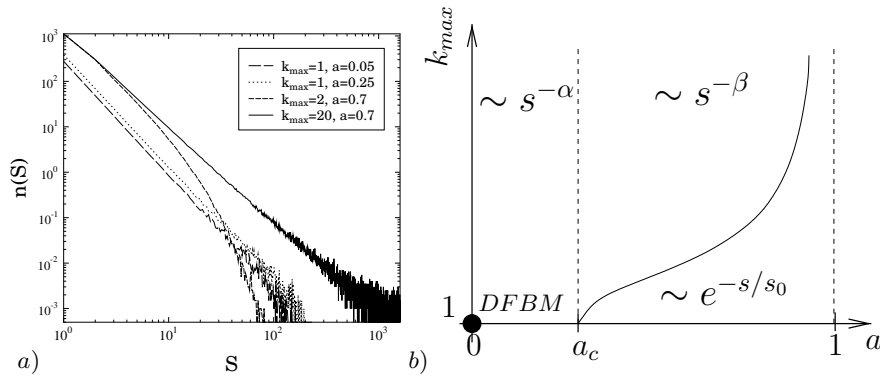


**Fig. 7.** a) Avalanche size distributions for different values of  $k_{max}$  and  $a$  when fibers have remaining stiffness and the disorder is annealed. The number of fibers was  $N = 1600$  and averages were made over 2000 samples. The number of avalanches  $D$  of size  $\Delta$  are shown to demonstrate also how the total number of avalanches changes. b) Phase diagram for the continuous damage model with remaining stiffness for both types of disorder. The functional form of the avalanche statistics is given in the parameter regimes. The location of DFBM in the parameter space is also indicated.

diagram is constructed which summarizes the properties of avalanches with respect to the parameters of the model. Fig. 7 demonstrates the existence of three different regimes. If the damage parameter  $a$  is smaller than  $a_c$ , the dynamics of avalanches is close to the simple DFBM characterized by a power law of the mean field exponent  $\alpha = 5/2$ . However, for  $a > a_c$  the avalanche size distribution depends on the number of failures  $k_{max}$  allowed. The curve of  $k_c(a)$  in the phase diagram separates two different regimes. For the parameter regime below the curve, avalanche distributions with an exponential shape were obtained. However, the parameter regime above  $k_c(a)$  is characterized by a power law distribution of avalanches with a constant exponent  $\beta = 2.12 \pm 0.05$  significantly different from the mean field exponent  $\alpha = 5/2$  [28, 22, 54]. It is important to emphasize that the overall shape of phase diagram is independent of the type of the disorder (annealed or quenched), moreover, the specific values  $a_c \approx 0.3$  and  $k_c(a)$  depend on the details of the disorder distribution  $p(\sigma_{th})$ .

## 4 Variable range of load sharing

In this section we introduce a one-parameter load transfer function to obtain a more realistic description of the interaction of fibers. Varying its parameter, the load transfer function interpolates between the two limiting cases of load redistribution, i.e. the global and the local load sharing schemes widely studied in the literature. We show that varying the effective range of interaction a crossover occurs from mean field to short range behavior. To explore the properties of the two regimes and the emergence of the crossover in between, a comprehensive numerical study of the model is performed. We study the dependence of the ultimate strength of the material on the system size and found that the system has only one nonzero critical point in the thermodynamic limit. When no critical point exists, the ultimate strength of the material goes to zero exactly as in local load sharing models as  $\sim 1/\ln(N)$ , with increasing system size  $N$ . We also study the distribution of avalanches and cluster sizes for the two distinct regimes and perform a moments analysis to accurately obtain the crossover value [26].

### 4.1 Load transfer function

The fracture of heterogeneous systems is characterized by the highly localized concentration of stresses at the crack tips that makes possible the nucleation of new micro-cracks at these regions leading to the growth of the crack and final failure of the system. In elastic materials, the stress distribution about cracks follows a power law

$$\sigma_{add} \sim r^{-\gamma}, \quad (13)$$

where  $\sigma_{add}$  is the stress increase on a material element at a distance  $r$  from the crack tip. Motivated by the above result of fracture mechanics we extend the fiber bundle model introducing a load sharing rule of the form of Eq. (13).

In the model we suppose that, in general, all intact fibers have a nonzero probability of being affected by the ongoing failure event, and that the additional load received by an intact fiber  $i$  depends on its distance  $r_{ij}$  from fiber  $j$  which has just been broken. Furthermore, elastic interaction is assumed between fibers such that the load received by a fiber follows the power law form. Hence, in our discrete model the stress-transfer function  $F(r_{ij}, \gamma)$  takes the form

$$F(r_{ij}, \gamma) = Z r_{ij}^{-\gamma}, \quad (14)$$

where  $\gamma$  is an adjustable parameter and  $r_{ij}$  is the distance of fiber  $i$  to the rupture point  $(x_j, y_j)$ , i.e.,  $r_{ij} = \sqrt{(x_i - x_j)^2 + (y_i - y_j)^2}$  in 2D.  $Z$  is given by the normalization condition  $Z = (\sum_{i \in I} r_{ij}^{-\gamma})^{-1}$ , where the sum runs over the set  $I$  of all intact elements. For simplicity, periodic boundary conditions with the minimum image convention are used (no Ewald summation is performed [1]) so that the largest  $r$  value is  $R_{max} = \frac{\sqrt{2}(L-1)}{2}$ , where  $L$  is the linear size of the system. It is easy to see that in the limits  $\gamma \rightarrow 0$  and  $\gamma \rightarrow \infty$  the load transfer function Eq. (14) recovers the two extreme cases of load redistribution of fiber bundle models, i.e. the global and the local load sharing, respectively. We should note here that, strictly speaking, for all  $\gamma$  different from the two limits above, the range of interaction covers the whole lattice. However, when changing the exponent, one moves from a very localized *effective* interaction to a truly global one as  $\gamma$  approaches zero. So, we will refer henceforth to a change in the *effective* range of interaction.

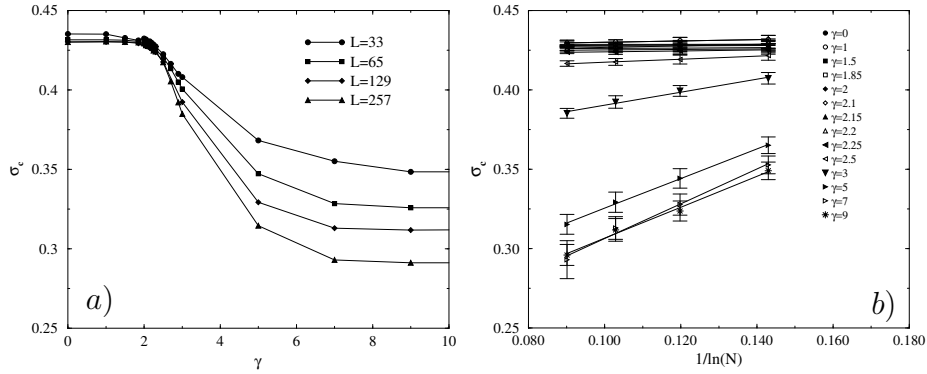


**Fig. 8.** *a)* Macroscopic strength  $\sigma_c$  of fiber bundles of different size  $L$  as a function of the exponent  $\gamma$  of the load transfer function Eq. (14). *b)* Variation of  $\sigma_c$  with the number of fibers of the bundle  $N$  at different  $\gamma$  values.

## 4.2 Macroscopic strength of bundles

We have carried out large scale computer simulations of the model described above in two dimensions. The fibers with Weibull distributed strength values Eq. (2) are organized on a square lattice of linear size  $L$  using periodic boundary conditions (see also Fig. 1). Computer simulations were performed varying the effective range of interaction  $\gamma$  over a broad interval recording the avalanche size distribution, the cluster size distribution and the ultimate strength of the bundle for several system sizes  $L$ . Each numerical simulation was repeated over at least 50 different realizations of the disorder distribution with the parameter values  $m = 2$  and  $\lambda = 1$  of the Weibull distribution.

Figure 8a) shows the ultimate strength  $\sigma_c$  of the fiber bundle for different values of the parameter  $\gamma$  and several system sizes from  $L = 33$  to  $L = 257$ . Clearly, two distinct regimes can be distinguished: For small  $\gamma$ , the strength  $\sigma_c$  is independent, within statistical errors, of both the effective range of interaction  $\gamma$  and the system size  $L$ . At a given point  $\gamma = \gamma_c$  a crossover is observed, where  $\gamma_c$  falls in the vicinity of  $\gamma = 2$ . The region  $\gamma > \gamma_c$  might eventually be further divided into two parts, the first region characterized by the dependence of the ultimate strength of the bundle on both the system size and the effective range of interaction; and a second region where  $\sigma_c$  only depends on the system size. This would mean that there might be two transition points in the model, for which the system displays qualitatively and quantitatively different behaviors. For  $\gamma \leq \gamma_c$  the ultimate strength of the bundle behaves as in the limiting case of global load sharing, whereas for  $\gamma \geq \gamma_c$  the local load sharing behavior seems to prevail. Nevertheless, the most important feature is that when decreasing the effective range of interaction in the thermodynamic limit, for  $\gamma > \gamma_c$ , the critical load is zero. This observation is further supported by Fig. 8b), where we have plotted the evolution of  $\sigma_c$  as a function of  $1/\ln N$  for different values of the exponent  $\gamma$ . Here, the two limiting cases are again clearly differentiated. For large  $\gamma$  all curves decrease when  $N \rightarrow \infty$  as

$$\sigma_c(N) \sim \frac{\alpha}{\ln N} \quad (15)$$

This qualifies for a genuine short range behavior as found in LLS models where the same relation was obtained for the asymptotic strength of the bundle [49]. It is worth noting that in the model we are analyzing, the limiting case of local load sharing corresponds to models in which short range interactions are considered to affect the nearest and the next-nearest neighbors. In the transition region, the maximum load the system can support also decreases as we approach the thermodynamic limit, but in this case much slower than for  $\gamma \gg \gamma_c$ . It has been pointed out that for some modalities of stress transfer, which can be considered as intermediate between GLS and LLS,  $\sigma_c$  decreases for large system sizes following the relation  $\sigma_c \sim 1/\ln(\ln N)$  as in the case of hierarchical load transfer models [41]. In our case, we have fitted our results with this relation but we have not obtained a single collapsed curve because

the slopes continuously vary until the LLS limit is reached. Finally, the region where the ultimate stress does not depend on the system size shows the behavior expected for the standard GLS model, where the critical load can be exactly computed as  $\sigma_c = (me)^{-1/m}$  for the Weibull distribution. The numerical values obtained for  $m = 2$  are in good agreement with this later expression.

### 4.3 Microstructure of damage

In order to characterize the fracture process under the quasistatically increasing external load we analyzed the cluster structure of broken fibers. The clusters formed during the evolution of the fracture process are sets of spatially connected broken sites on the square lattice [33, 70, 71]. We consider the clusters just before the global failure and they are defined taking into account solely nearest neighbor connections. As it has been discussed in Sec. 2, the case of global load sharing does not assume any spatial structure of fibers since it corresponds to the mean field approach. However, in our case it is obtained as a limiting case of a local load sharing model on a square lattice, which justifies the cluster analysis also for GLS. Fig. 9 illustrates how the cluster structure just before complete breakdown changes for various values of  $\gamma$ . In the limit where the long range interaction dominates, the clusters are randomly distributed on the lattice indicating that there is no correlated crack growth in the system as well as no stress concentration occurs. The cluster structure of the limiting case of  $\gamma = 0$  can be mapped to percolation clusters on a square lattice generated with the probability  $0 < P(\sigma_c) < 1$ , where  $\sigma_c$  is the fracture strength of the fiber bundle. However, the value of  $P(\sigma_c)$  depends on the Weibull exponent  $m$  Eq. (2) and is normally different from the critical percolation probability  $p_c = 0.592746$  of the square lattice. Equality  $P(\sigma_c) = p_c$  is obtained for  $m = 1.1132$ , hence, for physically relevant  $m$  values used in simulations, the system is below  $p_c$  at complete breakdown. This picture radically changes when the short range interaction prevails. In this case, the stress transfer is limited to a neighborhood of the failed elements and there appear regions where a few isolated cracks drive the rupture of the material by growth and coalescence. The differences in the structure of clusters also explain the lack of a critical strength when  $N$  goes to infinity in models with local stress redistribution. Since in the GLS model the clusters are randomly dispersed across the entire lattice, the system can tolerate a larger amount of damage and a higher stress, whereas for LLS models a small increment of the external field may provoke a run away event ending with the macroscopic breakdown of the material. All the above numerical results suggest that the crossover between the mean field and the short range regimes occurs in the vicinity of  $\gamma = 2$ . Further support for the precise value of  $\gamma_c$  can be obtained by studying the change in the cluster structure of broken fibers. The moments of  $n(s_c)$  defined as

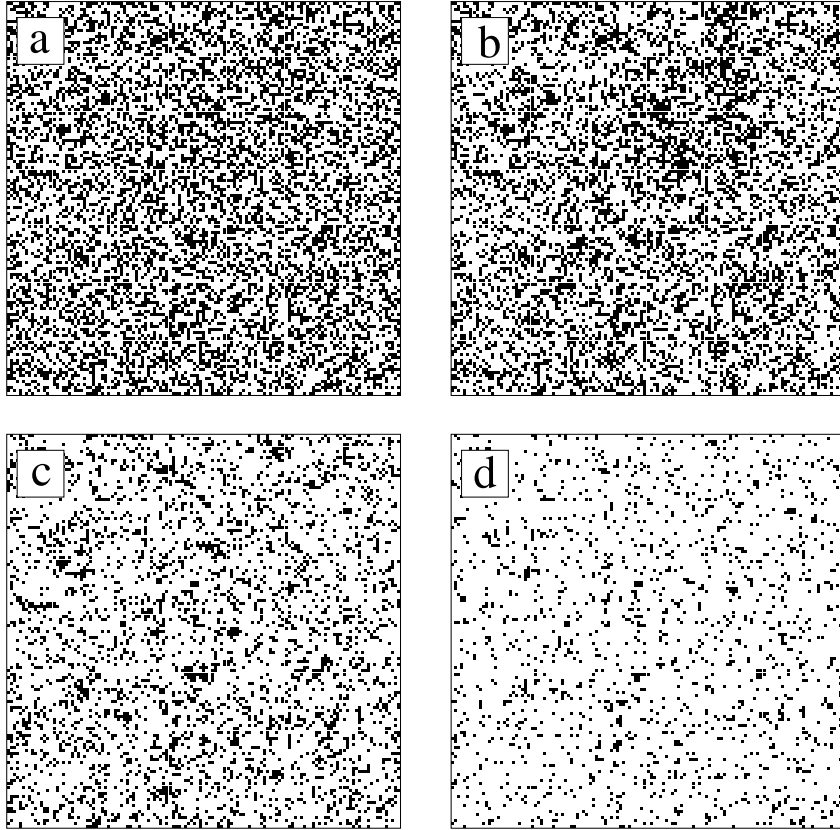


**Fig. 9.** Snapshots of the clusters of broken fibers (black dots) just before complete breakdown occurs. A clear change of the cluster structure can be observed. The values of  $\gamma$  are: *a*)  $\gamma = 0$ , *b*)  $\gamma_c = 2.2$ , *c*)  $\gamma = 3.0$ , and *d*)  $\gamma = 9.0$ .

$$m_k \equiv \int s_c^k n(s_c) ds \quad (16)$$

where  $m_k$  is the  $k$ th moment, describe much of the physics associated with the breakdown process. We study these moments to quantitatively characterize the point where the crossover from mean field to short range behavior takes place. The zero moment  $n_c = m_0$  is the total number of clusters in the system and is plotted in Fig. 10*a*) as a function of the parameter  $\gamma$ . Figure 10*b*) presents the variation of the first moment of the distribution  $m_1$ , which is equal to the total number of broken fibers  $N_c = m_1$ . It turns out that up to a certain value of the effective range of interaction  $\gamma$ ,  $N_c$  remains constant and then it decreases fast until a second plateau seems to arise. Note that the constant value of  $N_c$  for small  $\gamma$  is in agreement with the value of the

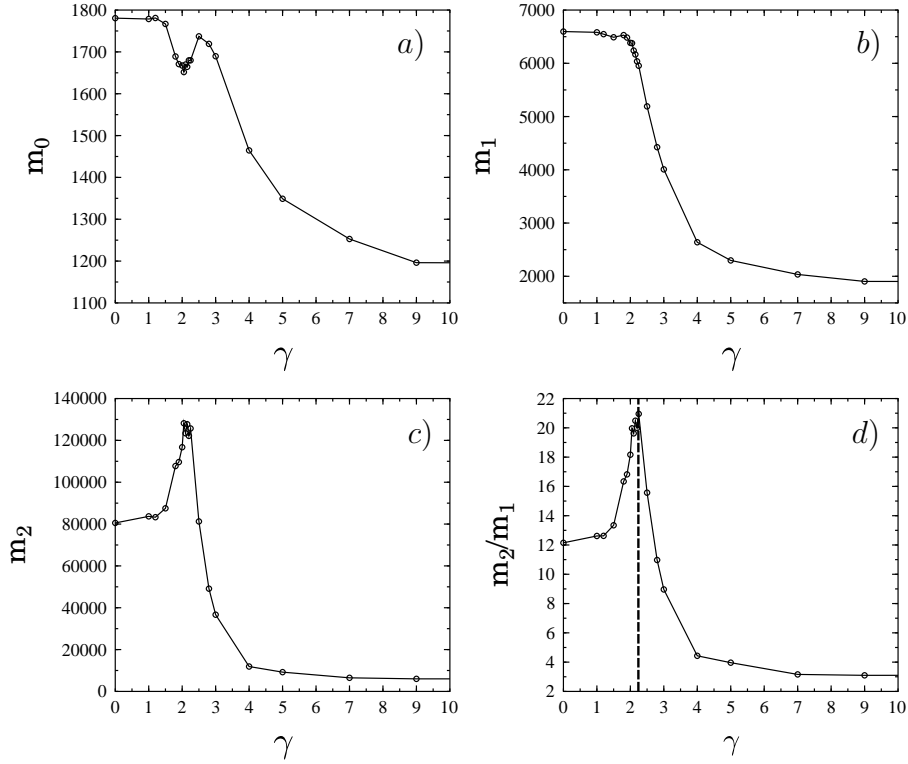


**Fig. 10.** Moments  $m_k$  of the clusters of broken fibers as a function of  $\gamma$ . The 0th and first moments are equal to the total number of clusters  $n_c = m_0$  (a) and the total number of broken fibers  $N_c = m_1$  (b), respectively. The average cluster size  $\langle s_c \rangle$  can be determined as the ratio of the second (c) and first moments  $\langle s_c \rangle = m_2/m_1$  (d).

fraction of broken fibers just before the breakdown of the material in mean field models [62, 33]. This property clearly indicates a change in the evolution of the failure process and may serve as a criterion to determine the crossover point. However, a more abrupt change is observed in the average cluster size  $\langle s_c \rangle$  as a function of  $\gamma$ . According to the moments description, the average cluster size is equal to the second moment of the cluster distribution divided by the total number of broken sites, *i.e.*  $\langle s_c \rangle = m_2/m_1$ . It can be seen in Fig. 10d) that  $\langle s_c \rangle$  has a sharp maximum at  $\gamma = 2.2 \pm 0.1$ , and thus the average cluster size drastically changes at this point, which again suggests the crossover point to be in the vicinity of  $\gamma_c = 2$ .

## 5 Damage enhanced creep in fiber bundles

Under high steady stresses, materials may undergo time dependent deformation resulting in failure called creep rupture which limits their lifetime, and hence, has a high impact on their applicability in construction elements. Creep failure tests are usually performed under uniaxial tensile loading when the specimen is subjected to a constant load  $\sigma_0$  and the time evolution of the damage process is followed by recording the strain  $\varepsilon$  of the specimen and the acoustic signals emitted by microscopic failure events. In order to describe the time dependent macroscopic response and finite lifetime of materials in the framework of FBMs, we extend the classical fiber bundle model presented in Sec. 2 by assuming that the fibers are viscoelastic, *i.e.* they exhibit time dependent deformation under a constant external load and fail in a strain controlled manner. In the framework of the viscoelastic fiber bundle model we show by analytical and numerical calculations that there exists a critical load above which the deformation of the system monotonically increases in time resulting in global failure at a finite time  $t_f$ , while below the critical load the deformation tends to a constant value giving rise to an infinite lifetime. Our studies revealed that for global load sharing the transition between the two regimes occurs analogously to continuous phase transitions, while for local load sharing it becomes abrupt, defining two universality classes of creep rupture [25, 31, 32].

### 5.1 Viscoelastic fiber bundle

In order to capture time dependent macroscopic response in the framework of fiber bundle models, we assume that the fibers themselves are viscoelastic. For simplicity, the pure viscoelastic behavior of fibers is modelled by a Kelvin-Voigt element which consists of a spring and a dashpot in parallel and results in the constitutive equation  $\sigma_0 = \beta \dot{\varepsilon} + E\varepsilon$ , where  $\sigma_0$  is the external load,  $\beta$  denotes the damping coefficient, and  $E$  is the Young modulus of fibers, respectively (see Fig. 11a)).

In order to capture failure in the model a strain controlled breaking criterion is imposed, *i.e.* a fiber fails during the time evolution of the system when its strain exceeds a breaking threshold  $\varepsilon_i, i = 1, \dots, N$  drawn from a probability distribution. For the stress transfer between fibers following fiber failure we assume that the excess load is equally shared by all the remaining intact fibers (global load sharing), which provides a satisfactory description of load redistribution in continuous fiber reinforced composites. For the breaking thresholds of fibers a uniform distribution Eq. (1) between 0 and 1, and a Weibull distribution Eq. (2) were considered. The construction of the model is illustrated in Fig. 11a). In the framework of global load sharing most of the quantities describing the behavior of the fiber bundle can be obtained analytically. In this case the time evolution of the system under a steady external load  $\sigma_0$  is described by the differential equation

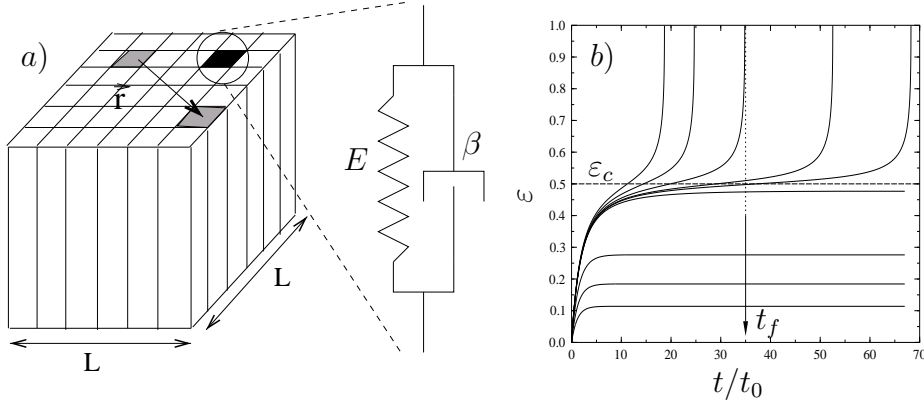


**Fig. 11.** *a)* The viscoelastic fiber bundle model. Intact fibers are modelled by Kelvin-Voigt elements. *b)*  $\varepsilon(t)$  for several different values of the external load  $\sigma_0$  below and above  $\sigma_c$ .  $t_0$  denotes the characteristic timescale of the system  $t_0 = \beta/E$ .

$$\frac{\sigma_0}{1 - P(\varepsilon)} = \beta \dot{\varepsilon} + E\varepsilon, \quad (17)$$

where the viscoelastic behavior is coupled to the failure of fibers [25, 31, 32].

## 5.2 Macroscopic response

The viscoelastic fiber bundle model with the equation of motion Eq. (17) can provide an adequate description of natural fiber composites like wood subjected to a constant load [15]. For the behavior of the solutions  $\varepsilon(t)$  of Eq. (17) two distinct regimes can be distinguished depending on the value of the external load  $\sigma_0$ : when  $\sigma_0$  falls below a critical value  $\sigma_c$ , Eq. (17) has a stationary solution  $\varepsilon_s$ , which can be obtained by setting  $\dot{\varepsilon} = 0$ , i.e.  $\sigma_0 = E\varepsilon_s[1 - P(\varepsilon_s)]$ . It means that as long as this equation can be solved for  $\varepsilon_s$  at a given external load  $\sigma_0$ , the solution  $\varepsilon(t)$  of Eq. (17) converges to  $\varepsilon_s$  when  $t \rightarrow \infty$ , and the system suffers only a partial failure. However, when  $\sigma_0$  exceeds the critical value  $\sigma_c$  no stationary solution exists, furthermore,  $\dot{\varepsilon}$  remains always positive, which implies that for  $\sigma_0 > \sigma_c$  the strain of the system  $\varepsilon(t)$  monotonically increases until the system fails globally at a finite time  $t_f$  [25, 31, 32].

The behavior of is illustrated in Fig. 11b) for several values of  $\sigma_0$  below and above  $\sigma_c$  with uniformly distributed breaking thresholds between 0 and 1. It follows from the above argument that the critical value of the load  $\sigma_c$  is the static fracture strength of the bundle. The creep rupture of the viscoelastic bundle can be interpreted so that for  $\sigma_0 \leq \sigma_c$  the bundle is partially damaged implying an infinite lifetime  $t_f = \infty$  and the emergence of a stationary macroscopic state, while above the critical load  $\sigma_0 \geq \sigma_c$  global failure

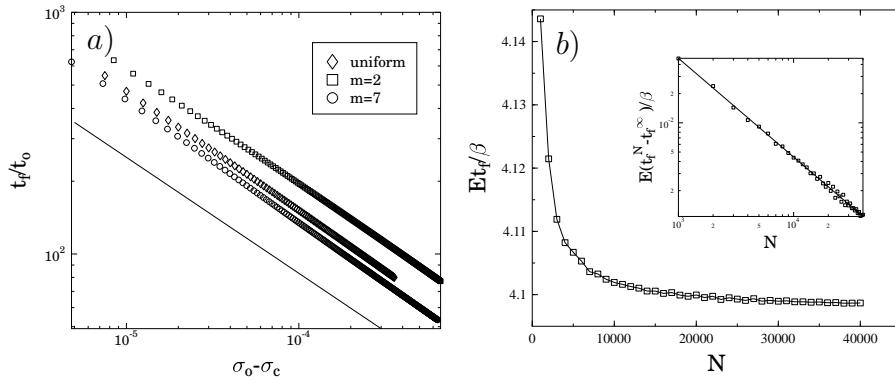


**Fig. 12.** *a)* Lifetime  $t_f$  of the bundle as a function of the distance from the critical point  $\sigma_0 - \sigma_c$  for three different disorder distributions, i.e. uniform distribution and Weibull distribution with  $m = 2$  and  $m = 7$  were considered. *b)*  $t_f$  as a function of the number of fibers  $N$  at a fixed value of the external load  $\sigma_0$ . Results of computer simulations (symbols) are in good agreement with the analytic predictions (solid lines).

occurs at a finite time  $t_f$ , but in the vicinity of  $\sigma_c$  the global failure is preceded by a long lived stationary state. The nature of the transition occurring at  $\sigma_c$  can be characterized by analyzing how the creeping system behaves when approaching the critical load both from below and above. For  $\sigma_0 \leq \sigma_c$ , the fiber bundle relaxes to the stationary deformation  $\varepsilon_s$  through a gradually decreasing breaking activity. It can be shown analytically that  $\varepsilon(t)$  has an exponential relaxation to  $\varepsilon_s$  with a characteristic time scale  $\tau$  that depends on the external load  $\sigma_0$  as

$$\tau \sim (\sigma_c - \sigma_0)^{-1/2}, \quad (18)$$

for  $\sigma_0 \leq \sigma_c$ , i.e. when approaching the critical point from below the characteristic time of the relaxation to the stationary state diverges according to a universal power law with an exponent  $1/2$  independent on the form of the disorder distribution  $P$ .

Above the critical point the lifetime defines the characteristic time scale of the system which can be cast in the form

$$t_f \sim (\sigma_0 - \sigma_c)^{-1/2}, \quad (19)$$

for  $\sigma_0 > \sigma_c$ , so that  $t_f$  also has a power law divergence at  $\sigma_c$  with a universal exponent  $1/2$  like  $\tau$  below the critical point, see Fig. 12a). Hence, for global load sharing the system exhibits scaling behavior on both sides of the critical point indicating a continuous transition at the critical load  $\sigma_c$ . It can also be shown analytically that fixing the external load above the critical point,

the lifetime  $t_f$  of the system exhibits a universal scaling with respect to the number  $N$  of fibers of the bundle (Fig. 12b)). The lifetime of finite bundles  $t_f^N$  decreases to the lifetime of the infinite bundle as  $t_f^N - t_f^\infty \sim 1/N$  [25, 31].

### 5.3 Microscopic damage process

The process of fiber breaking on the micro level can easily be monitored experimentally by means of the acoustic emission techniques. Except for the primary creep regime, where a large amount of fibers break in a relatively short time, the time of individual fiber failures can be recorded with a high precision. In order to characterize the process of fiber breaking in our viscoelastic fiber bundle model, we calculated numerically the distribution  $f$  of waiting times  $\Delta t$  between consecutive breaks [32]. A detailed analysis revealed that  $f(\Delta t)$  shows a power law behavior on both sides of the critical point

$$f(\Delta t) \sim \Delta t^{-b} \quad (20)$$

[32]. The value of the exponent  $b$  is different on the two sides of the critical point, *i.e.*  $b \approx 1.5$  and  $b \approx 2.0$  were measured below and above the critical load; however,  $b$  proved to be independent of the disorder distribution of fibers, see Fig. 13.

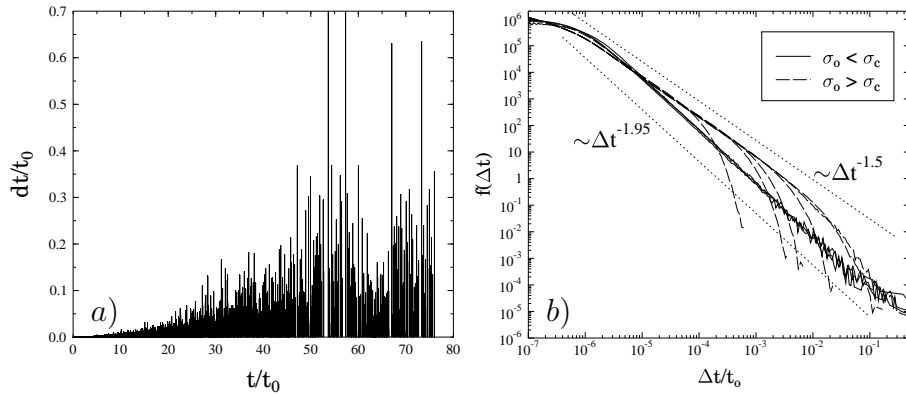


**Fig. 13.** *a)* Representative example of waiting times  $\Delta t$  between consecutive fiber breakings for a load  $\sigma_0 < \sigma_c$  plotted at the time  $t$  of breakings. *b)* Distribution  $f$  of  $\Delta t$  below and above the critical load. Simulation results are presented for  $10^7$  fibers with uniformly distributed threshold values between 0 and 1.

### 5.4 Universality classes of creep rupture

In order to clarify the effect of the range of load sharing on damage enhanced creep, we carried out computer simulations applying the variable range of load

sharing approach presented in Sec. 4 in the viscoelastic fiber bundle model (see also Fig. 11a) for explanation). Simulations were carried out varying the exponent  $\gamma$  of the load transfer function Eq. (14) in a broad range. Computer simulations revealed that the behavior described above for global load sharing prevails in the range  $0 \leq \gamma < \gamma_c$ , where the value of  $\gamma_c$  turned to be the same as the one determined in Sec. 4 for dry fiber bundles. For  $\gamma \geq \gamma_c$  the interaction of fibers becomes localized which results in an abrupt failure of the viscoelastic fiber bundle above the critical load  $\sigma_0 > \sigma_c$ , *i.e.* when  $\sigma_0$  exceeds  $\sigma_c$  the lifetime of the bundle suddenly jumps to a finite value without any scaling behavior. It is interesting to note, however, that the power law distribution of waiting times Eq. (20) prevails for localized load sharing. The value of the exponent  $b$  below the critical load  $\sigma_0 < \sigma_c$  is always  $b \approx 2.0$  independent of the effective range of load redistribution  $\gamma$ , while for  $\sigma_0 > \sigma_c$  the exponent  $b$  increases from  $\approx 1.5$  to  $\approx 2.0$  with increasing  $\gamma$  [32].

## 6 Failure of glued interfaces of solid blocks

Solid blocks are often joined together by welding or glueing of the interfaces which are expected to sustain various types of external loads. Besides welded joints, glued interfaces of solids play a crucial role in fiber reinforced composites where fibers are embedded in a matrix material. The properties of the fiber-matrix interface are controlled by the fabrication process of the composite and have an important effect on the mechanical performance of the system.

The classical setup of fiber bundle models have recently been applied to study the failure of glued interfaces when the external load is applied perpendicular to the interface of a rigid and a compliant block [4]. It was found that the compliance of one of the solid blocks introduces stress localization and results in a fractal structure of the failed glue just before macroscopic breakdown [4]. Glued interfaces can be teared apart by applying the external load locally at one of the ending point of the interface. Such loading conditions have also been studied in the framework of FBMs considering two stiff plates [29] and also the combination of a stiff plate and a compliant one [14, 13, 60].

In all the above studies, the external load resulted in a stretching deformation of material elements of the interface so that the classical fiber bundle model discussed in Sec. 1 provided an adequate framework for the theoretical description of the failure process. However, under shear loading more complex deformation states of material elements can arise leading to a more complex degradation process, which cannot be captured by FBMs. We propose a novel approach to the shear failure of glued interfaces by extending the classical fiber bundle model to model interfacial failure [58].

### 6.1 The beam model of interface failure under shear

In our model the interface is discretized in terms of elastic beams which can be elongated and bent when exposed to shear load, see Fig. 14. The beams are assumed to have identical geometrical extensions (length  $l$  and width  $d$ ) and linearly elastic behavior characterized by the Young modulus  $E$ . In order

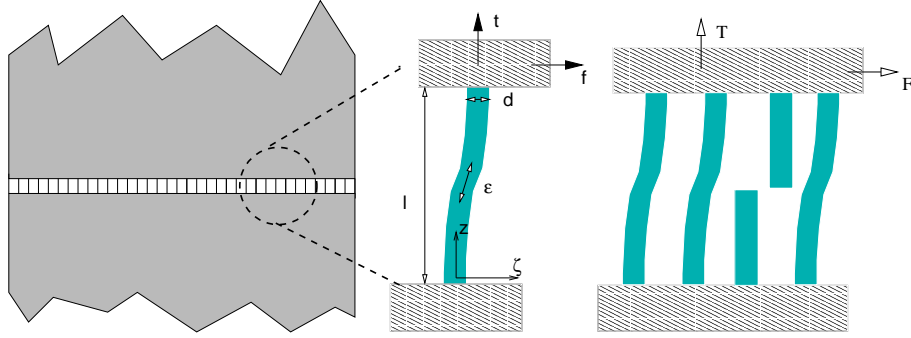


**Fig. 14.** Illustration of the model construction. The sheared interface is discretized in terms of beams (*left*), which suffer stretching and bending deformation (*middle*) and fail due to the two deformation modes (*right*).

to capture the failure of the interface, the beams are assumed to break when their deformation exceeds a certain threshold value. Under shear loading of the interface, beams suffer stretching and bending deformation resulting in two modes of breaking. The stretching and bending deformation of beams can be expressed in terms of a single variable, i.e. longitudinal strain  $\epsilon$ , which enables us to map the interface model to the simpler fiber bundle models. The two breaking modes can be considered to be independent or combined in the form of a von Mises type breaking criterion. The strength of beams is characterized by the two threshold values of stretching and bending a beam can withstand. The breaking thresholds are assumed to be randomly distributed variables of the joint probability distribution  $\rho$ . The randomness of the breaking thresholds is supposed to represent the disorder of the interface material. After breaking of a beam the excess load has to be redistributed over the remaining intact elements. Coupling to the rigid blocks ensures that all the beams have the same deformation giving rise to global load sharing, i.e. the load is equally shared by all the elements, stress concentration in the vicinity of failed beams cannot occur.

### 6.2 Constitutive behavior

Breaking of the beam is caused by two breaking modes, *i.e.* stretching and bending which can be either independent or coupled by an empirical breaking

criterion. Assuming that the two breaking modes are independent, a beam breaks if either the longitudinal stress  $t$  or the bending moment  $m$  exceeds the corresponding breaking threshold, see Fig. 14. Since the longitudinal stress  $t$  and the bending moment  $m$  acting on a beam can easily be expressed as functions of the longitudinal deformation  $\varepsilon$ , the breaking conditions can be formulated in a transparent way in terms of  $\varepsilon$ . To describe the relative importance of the breaking modes, we assign to each beam two breaking thresholds  $\varepsilon_1^i, \varepsilon_2^i$ ,  $i = 1, \dots, N$ , where  $N$  denotes the number of beams. The threshold values  $\varepsilon_1$  and  $\varepsilon_2$  are randomly distributed according to a joint probability density function  $p(\varepsilon_1, \varepsilon_2)$  between lower and upper bounds  $\varepsilon_1^{min}, \varepsilon_1^{max}$  and  $\varepsilon_2^{min}, \varepsilon_2^{max}$ , respectively. The density function needs to obey the normalization condition

$$\int_{\varepsilon_2^{min}}^{\varepsilon_2^{max}} d\varepsilon_2 \int_{\varepsilon_1^{min}}^{\varepsilon_1^{max}} d\varepsilon_1 p(\varepsilon_1, \varepsilon_2) = 1. \quad (21)$$

First, we provide a general formulation of the failure of a bundle of beams. We allow for two independent breaking modes of a beam that are functions  $f$  and  $g$  of the longitudinal deformation  $\varepsilon$ . Later on this case will be called the *OR* breaking rule. A single beam breaks if either its stretching or bending deformation exceed the respective breaking threshold  $\varepsilon_1$  or  $\varepsilon_2$ , i.e. failure occurs if

$$\frac{f(\varepsilon)}{\varepsilon_1} \geq 1, \quad \text{or} \quad (22)$$

$$\frac{g(\varepsilon)}{\varepsilon_2} \geq 1, \quad (23)$$

where Eqs. (22,23) describe the stretching and bending breaking modes, respectively. The failure functions  $f(\varepsilon)$  and  $g(\varepsilon)$  can be determined from the elasticity equations of beams, but in general the only restriction for them is that they have to be monotonous. For our specific case of sheared beams they take the form

$$f(\varepsilon) = \varepsilon, \quad g(\varepsilon) = a\sqrt{\varepsilon}, \quad (24)$$

where  $a$  is a constant and the value of the Young modulus  $E$  is set to 1. In the plane of breaking thresholds each point  $(\varepsilon_1, \varepsilon_2)$  represents a beam. For each value of  $\varepsilon$  those beams which survived the externally imposed deformation are situated in the area  $f(\varepsilon) \leq \varepsilon_1 \leq \varepsilon_1^{max}$  and  $g(\varepsilon) \leq \varepsilon_2 \leq \varepsilon_2^{max}$ , as it is illustrated in Fig. 15a). The constitutive behavior of the interface can be obtained by integrating the load of single beams over the intact ones in the plane of breaking thresholds in Fig. 15a). For the *OR* criterion one gets

$$\sigma = \varepsilon \int_{g(\varepsilon)}^{\varepsilon_2^{max}} d\varepsilon_2 \int_{f(\varepsilon)}^{\varepsilon_1^{max}} d\varepsilon_1 p(\varepsilon_1, \varepsilon_2). \quad (25)$$

Assuming the thresholds of the two breaking modes to be independently distributed, the disorder distribution factorizes  $p(\varepsilon_1, \varepsilon_2) = p_1(\varepsilon_1)p_2(\varepsilon_2)$  and  $\sigma(\varepsilon)$  takes the simple form

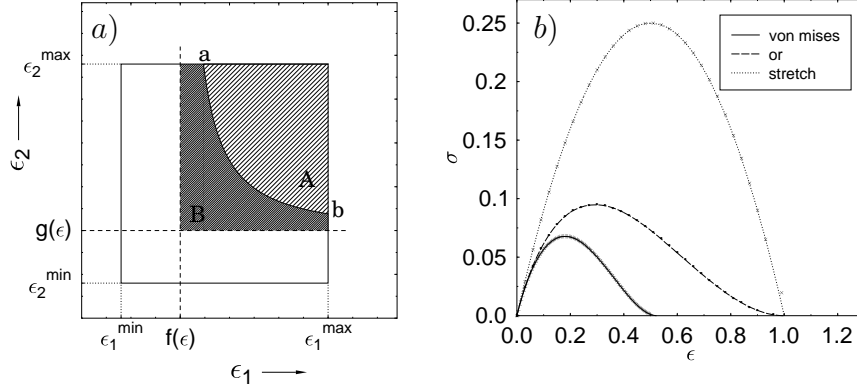


**Fig. 15.** *a)* The plane of breaking thresholds. Fibers which are intact at a deformation  $e$  fall in the rectangle bounded by and the maximum values of the two thresholds for the OR criterion (area A+B), and in the area bounded by the curve connecting  $a$  and  $b$  and the maximum thresholds for the von Mises type criterion (area A), respectively. The fibers which break due to the coupling of the two breaking modes in the von Mises criterion fall in area B. *b)* Comparison of the constitutive curves of a simple dry fiber bundle and of the beam model with different breaking criteria using uniformly distributed breaking thresholds.

$$\sigma = \epsilon[1 - P_1(f(\epsilon))][1 - P_2(g(\epsilon))]. \quad (26)$$

The terms  $1 - P_1(f(\epsilon))$  and  $1 - P_2(g(\epsilon))$  provide the fraction of beams failed under the stretching and bending breaking modes, respectively.

When the two breaking modes are coupled by a von Mises type breaking criterion, a single beam breaks if its strain  $\epsilon$  fulfils the condition

$$\left(\frac{f(\epsilon)}{\epsilon_1}\right)^2 + \frac{g(\epsilon)}{\epsilon_2} \geq 1. \quad (27)$$

This algebraic condition can be geometrically represented as it is illustrated in Fig. 15a). In this case the constitutive integral

$$\sigma = \epsilon \int_a^{\epsilon_1^{max}} d\epsilon_1 \int_{\tilde{\epsilon}_2(\epsilon_1, \epsilon)}^{\epsilon_2^{max}} d\epsilon_2 p(\epsilon_1, \epsilon_2) \quad (28)$$

cannot be performed explicitly with the integration limit  $\tilde{\epsilon}_2(\epsilon_1, \epsilon) = \epsilon_1^2 g(\epsilon) / (\epsilon_1^2 - f^2(\epsilon))$  in general so that  $\sigma(\epsilon)$  cannot be obtained in a closed analytic form. The constitutive curves obtained with the OR and von Mises breaking criteria are illustrated in Fig. 15b) for the specific case of a uniform distribution between  $\epsilon_1^{min} = \epsilon_2^{min} = 0$  and  $\epsilon_1^{max} = \epsilon_2^{max} = 1$ , *i.e.*  $P_1(\epsilon) = \epsilon$  and  $P_2(\epsilon) = \epsilon$ .

It follows from the structure of Eq. (26) and can be seen in Fig. 15b) that the existence of two breaking modes leads to a reduction of the strength of the

material, both the critical stress  $\sigma_c$  and strain  $\varepsilon_c$  take smaller values compared to the case of a single breaking mode applied in simple fiber bundle models [12, 62, 28, 26, 24, 37, 52, 5]. The coupling of the two breaking modes by the von Mises form Eq. (27) gives rise to further reduction of the interface strength. Note that due to the non-linearity of Eq. (27) also the functional form of  $\sigma(\varepsilon)$  changes.

### 6.3 Simulation techniques

Based on the above equations analytic results can only be obtained for the simplest forms of disorder like the uniform distribution. In order to determine the behavior of the system for complicated disorder distributions and explore the microscopic failure process of the sheared interface, it is necessary to work out a computer simulation technique. For the simulations we consider an ensemble of  $N$  beams arranged on a square lattice (see Fig. 1). Two breaking thresholds  $\varepsilon_1^i, \varepsilon_2^i$  are assigned to each beam  $i$  ( $i = 1, \dots, N$ ) of the bundle from the joint probability distribution  $p(\varepsilon_1, \varepsilon_2)$ . For the OR breaking rule, the failure of a beam is caused either by stretching or bending depending on which one of the conditions Eqs. (22,23) is fulfilled at a lower value of the external load. In this way an effective breaking threshold  $\varepsilon_c^i$  can be defined for the beams as

$$\varepsilon_c^i = \min(f^{-1}(\varepsilon_1^i), g^{-1}(\varepsilon_2^i)), \quad i = 1, \dots, N, \quad (29)$$

where  $f^{-1}$  and  $g^{-1}$  denote the inverse of  $f, g$ , respectively. A beam  $i$  breaks during the loading process of the interface when the load on it exceeds its effective breaking threshold  $\varepsilon_c^i$ . For the case of the von Mises type breaking criterion Eq. (27), the effective breaking threshold  $\varepsilon_c^i$  of beam  $i$  can be obtained as the solution of the algebraic equation

$$\left(\frac{f(\varepsilon_c^i)}{\varepsilon_1^i}\right)^2 + \frac{g(\varepsilon_c^i)}{\varepsilon_2^i} = 1, \quad i = 1, \dots, N. \quad (30)$$

In the case of global load sharing, the load and deformation of beams is everywhere the same along the interface, which implies that beams break in increasing order of their effective breaking thresholds. In the simulation, after determining  $\varepsilon_c^i$  for each beam, they are sorted in increasing order. Quasi-static loading of the beam bundle is performed by increasing the external load to break only a single element. Due to the subsequent load redistribution on the intact beams, the failure of a beam may trigger an avalanche of breaking beams. This process has to be iterated until the avalanche stops, or leads to catastrophic failure at the critical stress and strain.

In Fig. 15b) the analytic results on the constitutive behavior obtained with uniform distribution of the breaking thresholds are compared to the corresponding results of computer simulations. As a reference, we also plotted the constitutive behavior of a bundle of fibers where the fibers fail solely

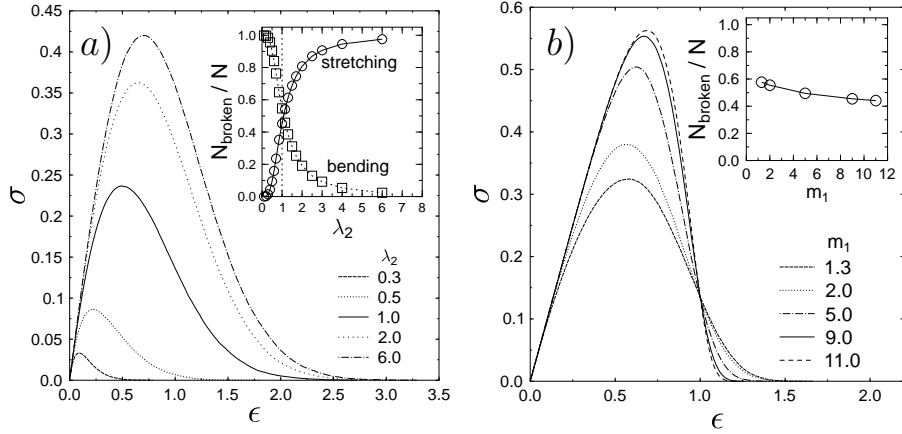


**Fig. 16.** *a)* Constitutive behavior of a bundle of  $N = 90000$  beams using the OR criterion for different values of the scale parameter  $\lambda_2$  of the bending mode. The other parameters were fixed  $m_1 = m_2 = 2.0$  and  $\lambda_1 = 1.0$ . Inset: fraction of beams broken under the two breaking modes. *b)* Constitutive behavior of the same bundle changing the Weibull exponent  $m_1$  of the stretching mode with  $\lambda_1 = \lambda_2 = 1.0$  and  $m_2 = 2.0$ . Inset: the fraction of beams broken under the bending mode.

due to simple stretching (*i.e.* DFBM) [12, 62, 28, 26, 24, 37, 52, 5]. It can be seen in the figure that the simulation results are in perfect agreement with the analytical predictions. It is important to note that the presence of two breaking modes substantially reduces the critical stress  $\sigma_c$  and strain  $\varepsilon_c$  ( $\sigma_c$  and  $\varepsilon_c$  are the value of the maximum of the constitutive curves) with respect to the case when failure of elements occurs solely under stretching [12, 62, 28, 26, 24, 37, 52, 5]. Since one of the failure functions is non-linear, the shape of the constitutive curve also changes, especially in the post-peak regime. The coupling of the two breaking modes in the form of the von Mises criterion gives rise to further reduction of the strength of the interface, see Fig. 15b).

#### 6.4 Microscopic damage process

During the quasi-static loading process of an interface, avalanches of simultaneously failing beams occur. Inside an avalanche, however, the beams can break solely under one of the breaking modes when the OR criterion is considered, or the breaking can be dominated by one of the breaking modes in the coupled case of the von Mises type criterion. In order to study the effect of the disorder distribution of beams on the relative importance of the two breaking modes and on the progressive failure of the interface, we considered independently distributed breaking thresholds both with a Weibull distribution of

exponents  $m_1$  and  $m_2$ , and scale parameters  $\lambda_1$  and  $\lambda_2$  for the stretching and bending modes, respectively. It can be seen in Fig. 16a) that increasing  $\lambda_2$  of the bending mode, the beams become more resistant against bending so that the stretching mode starts to dominate the breaking of beams, which is indicated by the increasing fraction of stretching failure. In the limiting case of  $\lambda_2 \gg \lambda_1$  the beams solely break under stretching. It is interesting to note that varying the relative importance of the two failure modes gives also rise to a change of the macroscopic constitutive behavior of the system. Shifting the strength distributions of beams, the functional form of the constitutive behavior remains the same, however, the value of the critical stress and strain vary in a relatively broad range. Varying the amount of disorder in the breaking thresholds, *i.e.* the Weibull exponents, has a similar strong effect on the macroscopic response of the system, see Fig. 16b). Applying the von Mises breaking criterion, the microscopic and macroscopic response of the interface show similar behavior (Fig. 17a)). Our careful numerical analysis of the microscopic failure process of the interface revealed that the size of avalanches of simultaneously failing beams under a stress controlled loading of the interface has a power law distribution (Fig. 17b)). The exponent of the power law proved to be  $5/2$ , it is equal to the mean field exponent characterizing the distribution of bursts in simple fiber bundle models [28].

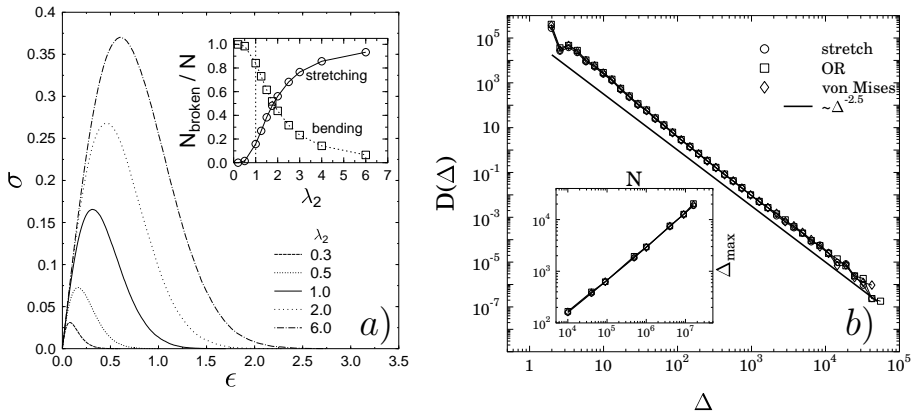


**Fig. 17.** *a)* Constitutive behavior of the interface applying the von Mises breaking criterion at different values of the scale parameter  $\lambda_2$  of the bending threshold. *b)* Comparison of the avalanche size distribution for the classical DFBM, the OR and the von Mises type breaking criteria. The inset shows that the size of largest avalanche  $\Delta_{max}$  is proportional to the size of the bundle  $N$ .

## 7 Discussion and outlook

We presented an overview of recent extensions of the classical fiber bundle model in order to provide a more description of the fracture and breakdown of disordered materials. We gradually improved the model by generalizing the damage law, constitutive behavior, deformation state and the way of interaction of the fibers. Analytical calculations and computer simulations have been carried out to explore the macroscopic response and the microscopic damage process of the extended model, which was then confronted with the classical FBM intensively studied in the literature.

Recently, several applications of the extended fiber bundle models have been proposed in a broad range of breakdown phenomena. The continuous damage fiber bundle model with the gradual degradation of fiber strength proved to adequately describe the relevant damage mechanism of various types of materials. CDFBM was successfully applied to understand the strength and fracture mechanism of nacre [44, 43], where even a quantitative comparison to experimental findings was possible. CDFBMs have also been considered to describe node breaking failures in scale free networks [38], and it has been further generalized considering time dependent fiber strength [34, 35].

An interesting study of the viscoelastic fiber bundle model was performed in Refs. [40, 39] where the model was further improved considering a more realistic time dependent response of single fibers instead of Kelvin-Voigt elements [40]. The authors carried out creep rupture experiments of fiber composites with randomly oriented short fibers and found a quantitative agreement of the model predictions and experimental results on the macro and micro behavior of the system [39]. The careful analyzes of the accumulation of damage in the viscoelastic fiber bundle model also helps to construct forecasting methods of the imminent macroscopic failure [64].

Based on the variable range of load sharing provided by the load transfer function Eq. (14), interesting results have recently been achieved on the analogy of damage and fracture to phase transitions and critical phenomena. Analyzing FBMs on scale free networks showed that besides the range of interaction also the structure of connectivity of the bundle is crucial to determine the universality class of the fracture transition [10]. Apart from fiber reinforced composites, short range interaction of fibers proved to be important also for the mechanical behavior and rupture of biological tissues [27].

*Acknowledgement.* This work was supported by the Collaborative Research Center SFB 381. F. Kun acknowledges financial support of the Research Contracts NKFP 3A-043/2004, OTKA M041537, T049209 and of the György Békésy Foundation of the Hungarian Academy of Sciences.

## References

1. M. P. Allen and D. J. Tildesley, editors. *Computer Simulation of Liquids*. Oxford University Press, Oxford, 1984.
2. J. V. Andersen, D. Sornette, and K. Leung. Tricritical Behaviour in Rupture Induced by Disorder. *Phys. Rev. Lett.*, 78:2140–2143, 1997.
3. G. G. Batrouni and A. Hansen. Fracture in three-dimensional fuse networks. *Phys. Rev. Lett.*, 80:325, 1998.
4. G. G. Batrouni, A. Hansen, and J. Schmittbuhl. Heterogeneous interfacial failure between two elastic blocks. *Phys. Rev. E*, 65:036126, 2002.
5. P. Bhattacharyya, S. Pradhan, and B. K. Chakrabarti. Phase transition in fiber bundle models with recursive dynamics. *Phys. Rev. E*, 67(14):046122, 2003.
6. B. K. Chakrabarti and L. G. Benguigui. *Statistical Physics of Fracture and Breakdown in Disordered Systems*. Oxford University Press, 1997.
7. B. D. Coleman. Time dependence of mechanical breakdown phenomena. *J. Appl. Phys.*, 27:862, 1956.
8. W. A. Curtin. The "tough" to brittle transition in brittle matrix composites. *J. Mech. Phys. Solids*, 41:217, 1993.
9. W. A. Curtin. Size Scaling of Strength in Heterogeneous Materials. *Phys. Rev. Lett.*, 80:1445–1448, 1998.
10. D.-H. Kim, B. J. Kim, and H. Jeong. Universality class of the fiber bundle model on complex networks. *Phys. Rev. Lett.*, 94:025501, 2005.
11. Ravá da Silveira. An introduction to breakdown phenomena in disordered systems. *Am. J. Phys.*, 67:1177, 1999.
12. H. E. Daniels. The Statistical Theory of the Strength of Bundles of Threads. I. *Proc. R. Soc London A*, 183:405–435, 1945.
13. A. Delaplace, S. Roux, and G. Pijaudier-Cabot. Damage cascade in a softening interface. *Int. J. Solids Struct.*, 36:1403–1426, 1999.
14. A. Delaplace, S. Roux, and G. Pijaudier-Cabot. Avalanche Statistics of Interface Crack Propagation in Fiber Bundle Model: Characterization of Cohesive Crack. *J. Eng. Mech.*, 127:646–652, 2001.
15. G. Dill-Langer, R. C. Hidalgo, F. Kun, Y. Moreno, S. Aicher, and H. J. Herrmann. Size dependency of tension strength in natural fiber composites. *Physica A*, 325:547–560, 2003.
16. A. G. Evans and F. W. Zok. The physics and mechanics of fibre-reinforced brittle matrix composites. *Journal of Materials Science*, 29:3857 – 3896, 1994.
17. J. B. Gómez, D. Iñiguez, and A. F. Pacheco. Solvable Fracture Model with Local Load Transfer. *Phys. Rev. Lett.*, 71:380, 1993.
18. A. Hansen and P. C. Hemmer. Burst Avalanches in Bundles of Fibers: Local Versus Global Load-Sharing. *Phys. Lett. A*, 184:394–396, 1994.
19. A. Hansen and S. Roux. Statistical toolbox for damage and fracture. In D. Krajcinovic and J. van Mier, editors, *Damage and Fracture of Disordered Materials*, number 410 in CISM Courses and Lectures, chapter 2, pages 17–101. Springer Verlag, 2000.
20. D. G. Harlow and S. L. Phoenix. The Chain-of-Bundles Probability Model For the Strength of Fibrous Materials i: Analysis and Conjectures. *J. Composite Materials*, 12:195, 1978.
21. D. G. Harlow and S. L. Phoenix. The Chain-of-Bundles Probability Model for the Strength of Fibrous Materials ii: A Numerical Study of Convergence. *J. Composite Materials*, 12:314, 1978.

22. P. C. Hemmer and A. Hansen. The Distribution of Simultaneous Fiber Failures in Fiber Bundles. *J. Appl. Mech.*, 59:909–914, 1992.
23. H. J. Herrmann and S. Roux, editors. *Statistical models for the fracture of disordered media*. Random materials and processes. Elsevier, Amsterdam, 1990.
24. R. C. Hidalgo, F. Kun, and H. J. Herrmann. Bursts in a fiber bundle model with continuous damage. *Phys. Rev. E*, 64(6):066122, 2001.
25. R. C. Hidalgo, F. Kun, and H. J. Herrmann. Creep rupture of viscoelastic fiber bundles. *Phys. Rev. E*, 65:032502, 2002.
26. R. C. Hidalgo, Y. Moreno, F. Kun, and H. J. Herrmann. Fracture model with variable range of interaction. *Phys. Rev. E*, 65:046148, 2002.
27. B. J. Kim. Phase transitions in the modified fiber bundle model. *Europhys. Letters*, 66:819, 2004.
28. M. Kloster, A. Hansen, and P. C. Hemmer. Burst avalanches in solvable models of fibrous materials. *Phys. Rev. E*, 56:2615–2625, 1997.
29. J. Knudsen and A. R. Massih. Breakdown of disordered media by surface loads. *Phys. Rev. E*, 72:036129, 2005.
30. F. Kun and H. J. Herrmann. Damage development under gradual loading of composites. *Journal of Materials Science*, 35:4685, 2000.
31. F. Kun, R. C. Hidalgo, H. J. Herrmann, and K. F. Pal. Scaling laws of creep rupture of fiber bundles. *Phys. Rev. E*, 67(6):061802, 2003.
32. F. Kun, Y. Moreno, R. C. Hidalgo, and H. J. Herrmann. Creep rupture has two universality classes. *Europhys. Lett.*, 63(3):347–353, 2003.
33. F. Kun, S. Zapperi, and H. J. Herrmann. Damage in fiber bundle models. *Eur. Phys. J. B*, 17:269, 2000.
34. L. Moral, J. B. Gomez, and Y. Moreno. Exact numerical solution for a time-dependent fibre-bundle model with continuous damage. *J. Phys. A-Math. Gen.*, 34:9983, 2001.
35. L. Moral, Y. Moreno, J. B. Gomez, and A. F. Pacheco. Time dependence of breakdown in a global fiber-bundle model with continuous damage. *Phys. Rev. E*, 63:066106, 2001.
36. Y. Moreno, J. B. Gómez, and A. F. Pacheco. Self-organized criticality in a fibre-bundle-type model. *Physica A*, 274:400, 1999.
37. Y. Moreno, J. B. Gomez, and A. F. Pacheco. Fracture and second-order phase transitions. *Phys. Rev. Lett.*, 85(14):2865–2868, 2000.
38. Y. Moreno, J. B. Gomez, and A. F. Pacheco. Instability of scale-free networks under node-breaking avalanches. *Eur. Phys. Lett.*, 58:630, 2002.
39. H. Nechad, A. Helmstetter, R. El Guerjouma, and D. Sornette. Andrade and critical time to failure laws in fiber-matrix composites: Experiments and model. *J. Mech. Phys. Solids*, 53:1099, 2005.
40. H. Nechad, A. Helmstetter, R. El Guerjouma, and D. Sornette. Creep ruptures in heterogeneous materials. *Phys. Rev. Lett.*, 94:045501, 2005.
41. W. I. Newman and A. M. Gabrielov. Failure of hierarchical distributions of fibre bundles. i. *International Journal of Fracture*, 50:1–14, 1991.
42. W. I. Newman, D. L. Turcotte, and A. M. Gabrielov. log-periodic behavior of a hierarchical failure model with applications to precursory seismic activation. *Phys. Rev. E*, 52:4827, 1995.
43. P. K. Nukala and S. Simunovic. A continuous damage random thresholds model for simulating the fracture behavior of nacre. *Biomaterials*, 26:6087, 2005.
44. P. K. Nukala and S. Simunovic. Statistical physics models for nacre fracture simulation. *Phys. Rev. E*, 72:041919, 2005.

45. P. V. V. Nukala, S. Simunovic, and S. Zapperi. Percolation and localization in the random fuse model. *J. Stat. Mech: Theor. Exp.*, page P08001, 2004.
46. F. T. Peires. Tensile tests for cotton yarns. v.-'the weakest link', theorems on the strength of long composite specimens. *J. Textile Inst.*, 17:T355–368, 1926.
47. S. L. Phoenix and I. J. Beyerlein. *Statistical Strength Theory for Fibrous Composite Materials*, volume 1 of *Comprehensive Composite Materials*, chapter 1.19, pages 1–81. Pergamon (Elsevier Science), 2000.
48. S. L. Phoenix, M. Ibnabdeljalil, and C.-Y. Hui. *Int. J. Solids Structures*, 34:545, 1997.
49. S. L. Phoenix and Beyerlein I. J. Statistical Strength Theory for Fibrous Composite Materials. In A. Kelly and C. Zweben, editors, *Comprehensive Composite Materials*, volume 1, chapter 1.19. Pergamon-Elsevier Science, New York, 2000.
50. S. L. Phoenix and R. Raj. Scalings in fracture probabilities for a brittle matrix fiber composite. *Acta metall. mater.*, 40:2813, 1992.
51. S. Pradhan and B. K. Chakrabarti. Precursors of catastrophe in the bak-tang-wiesenfeld, manna, and random-fiber-bundle models of failure. *Phys. Rev. E*, 65:016113, 2002.
52. S. Pradhan and B. K. Chakrabarti. Failure due to fatigue in fiber bundles and solids. *Phys. Rev. E*, 67(14):046124, 2003.
53. S. Pradhan and B. K. Chakrabarti. Failure properties of fiber bundle models. *Int. J. Mod. Phys. B*, 17:5565–5581, 2003.
54. S. Pradhan, A. Hansen, and P. C. Hemmer. Crossover behavior in burst avalanches: Signature of imminent failure. *Phys. Rev. Lett.*, 95:125501, 2005.
55. S. Pradhan, A. Hansen, and P. C. Hemmer. Crossover behavior in burst avalanches: Signature of imminent failure. *Phys. Rev. Lett.*, page 125501, 2005.
56. Srutarshi Pradhan and Alex Hansen. Failure properties of loaded fiber bundles having a lower cutoff in fiber threshold distribution. *Phys. Rev. E*, 72:026111, 2005.
57. S. R. Pride and R. Toussaint. Thermodynamics of fiber bundles. *Physica A*, 312:159–171, 2002.
58. F. Raischel, F. Kun, and H. J. Herrmann. Simple beam model for the shear failure of interfaces. *Phys. Rev. E*, 72:046126, 2005.
59. S. Roux. Thermally activated breakdown in the fiber-bundle model. *Phys. Rev. E*, 62:6164, 2000.
60. S. Roux, A. Delaplace, and G. Pijaudier-Cabot. Damage at heterogeneous interfaces. *Physica A*, 270:35–41, 1999.
61. R. Scorretti, S. Ciliberto, and A. Guarino. Disorder enhances the effect of thermal noise in the fiber bundle model. *Europhys. Lett.*, 55:626–632, 2001.
62. D. Sornette. Elasticity and failure of a set of elements loaded in parallel. *J. Phys. A*, 22:L243–L250, 1989.
63. D. Sornette. Mean-field solution of a block-spring model of earthquakes. *J. Phys. I. France*, 2:2089, 1992.
64. D. Sornette. Statistical physics of rupture in heterogeneous media. In S. Yip, editor, *Handbook of Materials Modeling*, chapter 4.4. Springer Science and Business Media, 2005.
65. D. Sornette and J. V. Andersen. Scaling with respect to disorder in time-to-failure. *Eur. Phys. J. B*, 1:353, 1998.
66. R. Toussaint and S. R. Pride. Interacting damage models mapped onto ising and percolation models. *Phys. Rev. E*, 71:046127, 2005.

67. D. L. Turcotte and M. T. Glasscoe. A damage model for the continuum rheology of the upper continental crust. *Tectonophysics*, 383:71–80, 2004.
68. E. Vives and A. Planes. Avalanches in a fluctuationless first-order phase transition in a random-bond ising model. *Phys. Rev. B*, 50:3839, 1994.
69. S. Zapperi, P. Ray, H. E. Stanley, and A. Vespignani. First-Order Transition in the Breakdown of Disordered Media. *Phys. Rev. Lett.*, 78:1408, 1997.
70. S. Zapperi, P. Ray, H. E. Stanley, and A. Vespignani. Analysis of damage clusters in fracture processes. *Physica A*, 270:57, 1999.
71. S. Zapperi, P. Ray, H. E. Stanley, and A. Vespignani. Avalanches in breakdown and fracture processes. *Phys. Rev. E*, 59:5049, 1999.
72. S. Zapperi, A. Vespignani, and H. E. Stanley. Plasticity and avalanche behaviour in microfracturing phenomena. *Nature*, 388:658, 1997.